

MODELLING CARBON DIOXIDE CONTENT OF A LIQUID DOMINATED
GEOTHERMAL RESERVOIR

A THESIS SUBMITTED TO
THE GRADUATE SCHOOL OF NATURAL AND APPLIED SCIENCES
OF
MIDDLE EAST TECHNICAL UNIVERSITY

BY

ALİ BERKAY TOKEL

IN PARTIAL FULFILLMENT OF THE REQUIREMENTS
FOR
THE DEGREE OF MASTER OF SCIENCE
IN
PETROLEUM AND NATURAL GAS ENGINEERING

DECEMBER 2023

Approval of the thesis:

**MODELLING CARBON DIOXIDE CONTENT OF A LIQUID
DOMINATED GEOTHERMAL RESERVOIR**

submitted by **ALİ BERKAY TOKEL** in partial fulfillment of the requirements for
the degree of **Master of Science in Petroleum and Natural Gas Engineering,**
Middle East Technical University by,

Prof. Dr. Halil Kalıpçılar
Dean, **Graduate School of Natural and Applied Sciences** _____

Assist. Prof. Dr. İsmail Durgut
Head of the Department, **Petroleum and Natural Gas
Engineering, METU** _____

Prof. Dr. Serhat Akin
Supervisor, **Petroleum and Natural Gas Engineering, METU** _____

Examining Committee Members:

Assist Prof. Dr. İsmail Durgut
Petroleum and Natural Gas Engineering, METU _____

Prof. Dr. Serhat Akin
Petroleum and Natural Gas Engineering, METU _____

Assist. Prof. Dr. Selçuk Erol
Energy Systems Engineering, IZTECH _____

Date: 11.12.2023

I hereby declare that all information in this document has been obtained and presented in accordance with academic rules and ethical conduct. I also declare that, as required by these rules and conduct, I have fully cited and referenced all material and results that are not original to this work.

Name Last name : Ali Berkay Tokel

Signature :

ABSTRACT

MODELLING CARBON DIOXIDE CONTENT OF A LIQUID DOMINATED GEOTHERMAL RESERVOIR

Tokel, Ali Berkay
Master of Science, Petroleum and Natural Gas Engineering
Supervisor : Prof. Dr. Serhat Akın

December 2023, 76 pages

Geothermal energy is a renewable and clean energy source that can be used for electricity generation. The share of geothermal energy in the electricity production in Turkey has been increasing steadily with recent incentives imposed by the state. Geothermal reservoirs in Menderes and Gediz grabens of Turkey naturally contain significant amounts of carbon dioxide. Carbon dioxide content of a reservoir considerable effects the electricity generation due to its impact on flashing point of the brine. Although the carbon dioxide content in the reservoir may be beneficial for electricity generation, emission of carbon dioxide from these power plants has negative effect on the environment. For these reasons, some portion of the carbon dioxide produced from the Kızıldere Geothermal Field was reinjected back into reservoir to mitigate emissions as part of Geothermal Emissions CONTROL (GECO) Project. To assess the safety and feasibility of the carbon dioxide reinjection, reservoir carbon dioxide levels and soil carbon dioxide fluxes were monitored. In this study, a lumped parameter model that can account for carbon dioxide content and soil carbon dioxide fluxes is developed. The developed model relates the soil

fluxes to the carbon dioxide content of the reservoir by a parameter (θ). The model developed in this study is fine-tuned using field observations, including data on pressure, carbon dioxide content, and soil carbon dioxide fluxes. Through this calibration process, the parameter θ is established to be 10.8×10^{-6} . The model is then utilized to forecast the carbon dioxide content in the pilot reinjection area over a period of five years under various carbon dioxide reinjection strategies. If the current operational parameters are maintained (no carbon dioxide reinjection), the carbon dioxide mass fraction in the study area is projected to decrease to 0.0115 over five years. For scenarios involving reinjection of water with 1 and 1.5 weight percent carbon dioxide, the predicted carbon dioxide contents after five years are 0.0121 and 0.0123, respectively.

Keywords: Geothermal Energy, Lumped Parameter Modelling, Kızıldere, Soil Carbon Dioxide Flux

ÖZ

SIVI HAKİM JEOTERMAL REZERVUARLARDA KARBON DİOKSİT İÇERİĞİNİN MODELLENMESİ

Tokel, Ali Berkay
Yüksek Lisans, Petrol ve Doğal gaz Mühendisliği
Tez Yöneticisi: Prof. Dr. Serhat Akın

Aralık 2023, 76 sayfa

Jeotermal enerji, elektrik üretimi için kullanılabilen yenilenebilir ve temiz bir enerji kaynağıdır. Türkiye'deki elektrik üretiminde jeotermal enerjinin payı, devlet tarafından uygulanan son teşviklerle artmaktadır. Türkiye'deki Menderes ve Gediz grabenlerindeki jeotermal rezervuarlar doğal olarak önemli miktarda karbondioksit içermektedir. Bir rezervuarın karbondioksit içeriği, jeotermal suyun flaş noktası üzerindeki etkisi nedeniyle elektrik üretimi üzerinde önemli etkilere sahiptir. Rezervuardaki karbondioksit içeriği elektrik üretimi için yararlı olsa da, bu santrallerden karbondioksit emisyonunun çevre üzerinde olumsuz etkileri vardır. Bu olumsuz etkileri azaltmak için, Jeotermal Emisyon Kontrol (GECO) projesi kapsamında Kızıldere Jeotermal Sahası'ndan üretilen karbondioksitin bir kısmı 5 ay boyunca tekrar rezervuara enjekte edilmiştir. Karbondioksit enjeksiyonunun güvenliğini ve uygulanabilirliğini değerlendirmek için rezervuar karbondioksit seviyeleri ve toprak karbondioksit akıları izlenmiştir. Bu çalışmada, karbondioksit içeriğini ve toprak karbondioksit akılarını hesaba katabilen bir boyutsuz parametre modeli geliştirilmiştir. Geliştirilen model, rezervuarın karbondioksit içeriğini bir parametre (θ) ile toprak akılarına bağlamaktadır. Bu çalışmada geliştirilen model, basınç, rezervuar karbondioksit içeriği ve toprak karbondioksit akışlarına dair alan

gözlemleri kullanılarak kalibre edilmiştir. Bu kalibrasyon süreciyle, θ parametresi 10.8×10^{-6} olarak belirlenmiştir. Model, daha sonra çeşitli karbondioksit enjeksiyon stratejileri altında pilot enjeksiyon alanındaki karbondioksit içeriğini beş yıl boyunca tahmin etmek için kullanılmıştır. Mevcut işletme parametreleri korunursa (karbondioksit enjeksiyonu yapılmazsa), çalışma alanındaki karbondioksit kütle fraksiyonunun beş yıl içinde 0.0115'e düşmesi beklenmektedir. %1 ve %1,5 ağırlık oranında karbondioksit ile enjekte edilen su senaryoları için, beş yıl sonra tahmin edilen karbondioksit içerikleri sırasıyla 0.0121 ve 0.0123'tür.

Anahtar Kelimeler: Jeotermal Enerji, Boyutsuz Parametre Modelleri, Kızıldere, Toprak Karbon Dioksit Akısı

To my beloved mother and sisters.

ACKNOWLEDGMENTS

I would like to express my deepest gratitude to my supervisor Prof. Dr. Serhat Akın for his guidance, encouragements, and insight throughout this research.

I would like to extend my gratitude to Dr. Selçuk Erol, Dr. Taylan Akın, and Dođuhan Barlas Sevindik for their help in collection, analysis, and conceptualization of soil flux measurements.

Lastly, I would like to thank Zorlu Energy for providing data for Kızıldere Geothermal Field.

This work has received funding from the European Union's Horizon 2020 Research and Innovation programme under Grant Agreement No. 818169-GECO.

TABLE OF CONTENTS

ABSTRACT.....	v
ÖZ.....	vii
ACKNOWLEDGMENTS.....	x
TABLE OF CONTENTS.....	xi
LIST OF TABLES.....	xii
LIST OF FIGURES.....	xiii
LIST OF ABBREVIATIONS.....	xv
LIST OF SYMBOLS.....	xvi
1 INTRODUCTION.....	1
2 LITERATURE REVIEW.....	5
3 STATEMENT OF THE PROBLEM.....	11
4 DESCRIPTION OF THE MODEL.....	13
5 MODELLING CARBON DIOXIDE CONTENT OF KIZILDERE GEOHERMAL FIELD.....	31
6 CONCLUSIONS AND FUTURE REMARKS.....	67
REFERENCES.....	71

LIST OF TABLES

TABLES

Table 4-1 Parameters used in lumped parameter model.	26
Table 4-2 Parameters used in analytical solution.	26
Table 5-1 Descriptive statistics for the August 2022 soil carbon dioxide flux measurements conducted at Kızıldere.	42
Table 5-2 Descriptive statistics of the March 2023 soil carbon dioxide flux measurements at Kızıldere.	45
Table 5-3 Estimated parameters of partitioned populations for August 2022 measurements.	54
Table 5-4 Estimated parameters of partitioned populations for March 2023 measurements.	54
Table 5-5 Soil flux rates calculated from anomalous populations:	55
Table 5-6 The tank parameters obtained from the history matching process.....	57

LIST OF FIGURES

FIGURES

Figure 4-1 A generalized lumped parameter (tank) model comprising of n tanks of which can make n-1 connections.	14
Figure 4-2 An example tank configuration for modelling a geothermal system. ...	15
Figure 4-3 Connectivity matrix for the given example tank configuration.	15
Figure 4-4 Flow chart of the solution algorithm.	24
Figure 4-5 Comparison of Analytical and Numerical Solution	27
Figure 5-1 Carbon dioxide reinjection design for well KD50A (Akin et al., 2023)	32
Figure 5-2 Detailed conceptual model of Kızıldere Geothermal Field and geological setting (modified as per the adaptations from Şimşek et al., 2009).	34
Figure 5-3 Area covered by the sector model for the Kızıldere Geothermal Field.	35
Figure 5-4 The two-tank configuration for the sector model.	35
Figure 5-5 Total production-reinjection history of sector model area.	36
Figure 5-6 Simulated and Observed Pressures for the reservoir tank.	38
Figure 5-7 Simulated and flow averaged dissolved carbon dioxides.	40
Figure 5-8 August 2022 measurement locations, wells, and faults.	42
Figure 5-9 August 2022 point-based soil carbon dioxide flux results	43
Figure 5-10 Cumulative Probabilities vs logarithm fluxes of the August 2022 soil flux measurements	44
Figure 5-11 Soil carbon dioxide flux results of March 2023 measurements.	46
Figure 5-12 Cumulative Probabilities vs logarithm fluxes of the March 2023 soil flux measurements	47
Figure 5-13 Averages of soil carbon dioxide flux measurements from Kızıldere Geothermal Field.	48
Figure 5-14 Location based comparison of soil fluxes between March 2019 and March 2023 measurements.	48
Figure 5-15 Comparison of soil flux, soil temperature and humidity measured at location 1 which is near the reinjection well.	49

Figure 5-16 Comparison of soil flux, soil temperature and humidity measured at location 22 which is between the first fault outcrop and the reinjection well.	50
Figure 5-17 Comparison of soil flux, soil temperature and humidity measured at location 53 which is located at second fault outcrop.....	50
Figure 5-18 Comparison of soil flux, soil temperature and humidity measured at location 42 which is located at first fault outcrop.	51
Figure 5-19 Probability plots and partitioning of August 2022 soil flux measurements.	53
Figure 5-20 Probability plots and partitioning of March 2023 soil flux measurements.	54
Figure 5-21 Sensitivity analysis of theta parameter for history matching of carbon dioxide soil flux rates.	56
Figure 5-22 The total production and reinjection rates for the scenarios investigated.....	58
Figure 5-23 Dissolved carbon dioxide mass fraction at the reservoir after five years.	59
Figure 5-24 Soil flux rates out from the reservoir tanks for scenario 1.	60
Figure 5-25 Dissolved carbon dioxide mass fraction at the reservoir after five years.	61
Figure 5-26 Soil flux rates from the reservoir tanks for scenario 2.....	62
Figure 5-27 Dissolved carbon dioxide mass fraction at the reservoir after five years.	63
Figure 5-28 Soil flux rates out from the reservoir tank for scenario 3.....	64
Figure 5-29 Comparison of scenarios with respect to the carbon dioxide content of the reservoir.....	65

LIST OF ABBREVIATIONS

ABBREVIATIONS

b(subscript): bulk

cl(subscript): dissolved carbon dioxide in liquid

inj(subscript): injection

p(subscript): production

w(subscript): water

m(subscript): rock matrix

re(subscript): recharge

LIST OF SYMBOLS

SYMBOLS

V_b : Bulk volume, m^3

P : Pressure, bar

T : Temperature, Celsius

f_{cl} : Dissolved carbon dioxide mass fraction, fraction

W_p : Production rate, $kg\ s^{-1}$

W_{inj} : Injection rate, $kg\ s^{-1}$

w_n : Number of wells

ϕ : Porosity, fraction

α : Recharge index, $kg\ bar^{-1}\ s^{-1}$

ρ : Density, $kg\ m^{-3}$

u : Specific internal energy, $J\ kg^{-1}$

C_m : Specific heat capacity of rock matrix

h : Specific enthalpy, $J\ kg^{-1}$

J : Jacobian matrix

w : solution vector

\mathbf{R} : Residual vector

R : Gas constant

N_t : Total number of tanks in the system

f_0 : Initial carbon dioxide mass fraction, fraction

F_c : Soil carbon dioxide flux rate, $\mu mol\ m^{-2}\ s^{-1}$

S : Soil surface area, cm^2

$C_c/\partial t$: Rate of change of carbon dioxide mole fraction, $\mu mol\ mol^{-1}$

CHAPTER 1

INTRODUCTION

Geothermal energy is the heat contained in Earth and its internal fluids. Geothermal energy is a renewable source since its source is the natural heat generated at Earth's core. Geothermal energy stands as a significant renewable energy source due to its continuous availability, low environmental impact, and long operational span.

Environmental concerns related to geothermal energy are low compared to the traditional energy sources like fossil fuels, although one of the primary issues related with the geothermal energy is the emission of non-condensable gases (NCGs) into the atmosphere. Non-condensable gases in geofluids consist of carbon dioxide, hydrogen sulfide, methane, nitrogen, argon, and other trace gases. Carbon dioxide typically constitutes a significant fraction (> %95) of the non-condensable gases.

In the process of generating electricity from geothermal reservoirs that naturally contain high levels of carbon dioxide, there can be significant emissions of carbon dioxide into the atmosphere. This phenomenon is observed for example in power plants situated in the Menderes and Gediz grabens in Turkey, Mount Amiata in Italy, and Ngawha in New Zealand (Fridriksson et al., 2016).

Although it is observed that carbon dioxide emissions from power plants situated in Menderes and Gediz grabens decline gradually with time (Akin et al., 2020), the management of carbon dioxide emissions in geothermal energy production has become increasingly important, as these emissions contribute to climate change. Geothermal Emission COntrol (GECO) project aims to address this issue and minimize the amount of carbon dioxide emitted on the fields around Europe. In the framework of the project, the emitted carbon dioxide is reinjected into the reservoir

as a method of reducing carbon dioxide emissions to the atmosphere similar to the CarbFix method carried out in Iceland.

To assess the safety and feasibility of the implemented carbon capture and storage scheme, it is crucial to monitor the movement of the injected carbon dioxide to ensure reinjected carbon dioxide is not emitted back. Potential mechanisms that could result in carbon dioxide being emitted back into the atmosphere include: the escape of carbon dioxide through the wellbore due to leakage, and the escape of carbon dioxide through permeable zones, such as faults.

In this context, a comprehensive monitoring campaign is initiated for reinjected carbon dioxide at Kızıldere Geothermal Field. The aim of this campaign is to provide insights on the behavior of reinjected carbon dioxide. The monitoring tools utilized for GECO demonstration site at Kızıldere are numerical reactive transport simulations, tracer tests, and soil flux measurements. These tools are utilized to assess the safety and feasibility of the pilot carbon dioxide reinjection project.

Soil carbon dioxide flux measurements are useful in monitoring for leaks from the subsurface reservoir. Soil flux measurements are utilized in many carbon capture and storage sites around the world as a mean of ensuring the safety of operation. At the Ketzin carbon dioxide storage site, a total of 67 kilotons (kt) of carbon dioxide were injected into a saline aquifer from June 2008 to August 2013 (Szizybalski et al., 2017). Soil carbon dioxide flux measurements were a part of the comprehensive monitoring program. Soil carbon dioxide fluxes at 20 long-term sampling locations were continuously recorded for twelve years. Comparison of mean values of soil carbon dioxide fluxes prior to the injection and after showed no indication of migration of injected carbon dioxide to the surface.

In a manner similar to the Ketzin carbon dioxide storage site, the Illinois Basin – Decatur Project (IBDP) saw the injection of approximately 1.1 million tonnes of carbon dioxide into a saline aquifer over the period from November 2011 to November 2014. Soil carbon dioxide flux measurements were a part of the IBDP monitoring, verification and accounting (MVA) program. Preliminary analysis on

soil flux measurements showed no carbon dioxide leakage from saline aquifer (Carman et al., 2014).

Measurements of soil carbon dioxide flux are also part of the monitoring of the pilot carbon dioxide reinjection at Kızıldere Geothermal Field. To monitor for leaks, it's important to establish baseline soil fluxes before the start of reinjection process. After the reinjection starts, soil flux measurements can then be compared to evaluate the feasibility of the reinjection. In 2019, six point-based soil carbon dioxide flux measurements were carried out during the months of February, March, April, June, September, and December, as reported by Küçük et al. (2021). Two additional sets of measurements were collected in August 2022 (Tokel et al., 2023), and March 2023 (Akın et al., 2023).

The methodology employed for monitoring soil fluxes at the Ketzin and Illinois Basin Decatur Project (IBDP) differs from that used in the Kızıldere pilot carbon dioxide reinjection project, primarily in that measurements at Ketzin and IBDP are conducted on a continuous basis.

Origin of the carbon dioxide flux from the soil can be attributed to biogenic processes such as respiration of plants, carbon dioxide generated by the decomposition of organic compounds, and oxidation of organic matter, or can be attributed to Earth's degassing (Camarda et al., 2019). After steam, carbon dioxide represents the primary volatile emitted from geothermal systems having medium to high enthalpy. In these systems, steam and carbon dioxide can escape through faults from deep reservoirs and ascend towards the surface. During this process, the steam generally condenses due to low temperatures, whereas carbon dioxide may reach to the surface (Carapezza et al., 2015). Consequently, soil carbon dioxide measured at a point is a combination of carbon dioxide fluxes emanating from different sources. Statistical methods are employed to determine the proportion of measured soil carbon dioxide fluxes that can be attributed to their respective sources of origin.

The primary objective of this study is to develop a model that establishes a connection between the soil carbon dioxide fluxes measured at the surface and the

carbon dioxide content in the subsurface reservoir, using a specific parameter which relates the carbon dioxide content of the reservoir to soil flux rates. This model aims to enable the quantification of any potential leaks and will be instrumental in clarifying the relationship between the subsurface reservoir's carbon dioxide levels and the surface soil flux measurements.

CHAPTER 2

LITERATURE REVIEW

2.1 Geothermal Reservoir Modelling

Reservoir modeling is a crucial aspect of both geothermal and oil and gas industries for effective reservoir development and management. In all reservoir simulation applications, the main goal is to understand and predict the behavior of the fluids of interest in the subsurface reservoir. The fluids of interest we're concerned with differ in petroleum reservoirs, its hydrocarbons, while in geothermal reservoirs, its water and any accompanying non-condensable gases.

Reservoir modeling aids in characterizing and comprehending subsurface reservoir conditions, facilitating effective development and utilization of the resource that lies underground. The absence of a robust reservoir model could impede accurate production forecasts, potentially resulting in economic losses due to the substantial costs associated with drilling wells, and commissioning power plants.

Various methodologies have been employed in the field of production forecasting and reservoir modeling. The development of reservoir simulation has closely followed advancements in computer technology, because the governing equations for subsurface porous medium flow being comprised of partial differential equations that lack exact analytical solutions. In general, three main strategies are commonly employed in the modelling of geothermal reservoirs. The first approach involves utilizing decline curve analysis (DCA), whereas subsequent two strategies consist of using either lumped parameter models or distributed parameter models (numerical models).

2.1.1 Decline Curve Analysis

The decline curve analysis serves as a straightforward and foundational method in production forecasting. The core concept involves fitting the historical production data from a reservoir into a mathematically describable curve which is subsequently employed to predict future production. Notably, Arps's study (1945) introduced exponential, hyperbolic and harmonic models that capture distinct patterns of production decline. While Arps's study focuses on petroleum industry, the principles of decline curve analysis can be extended to the field of geothermal reservoir engineering. The agreement between reserve estimates from decline curve analysis and results from mass balance studies was well observed at Larderello (Atkinson et al., 1978). Also, Ripperda and Bodvarsson (1987) identified a nearly harmonic decline behavior in the Geysers Field and used this to make predictions about production decline. The limitations of decline curve analysis are that it lacks geological insights and relies on robust production data. Also, changes in operations at the field can substantially impact reservoir behavior and, in turn, affect the predictive accuracy of decline curves.

2.1.2 Numerical Models

Numerical models for geothermal reservoirs are distributed parameter models. These models divide the geothermal reservoir into discrete grids, with each grid cell assigned unique properties like pressure, temperature, permeability, and fluid characteristics. By applying numerical techniques, the governing partial differential equations for these properties are solved for each grid cell. This approach effectively accounts for factors like reservoir geology, reservoir geometry, fluid properties, and operational conditions, resulting in reliable outcomes. However, it's important to note that numerical models demand extensive amounts of data, making them less suitable for newly developed fields with limited information available.

One of the widely used numerical simulators in geothermal reservoir engineering is TOUGH2 (Transport of Unsaturated Groundwater and Heat) (Pruess, 1991). It's a suite of computational tools designed to model fluid and heat flow below the surface in both porous and fractured media. TOUGH2 stands out for its ability to handle different fluid compositions. For example, it's well-equipped to simulate situations where geothermal water contains varying levels of carbon dioxide.

Subsequent additions to TOUGH have endowed it with the capability for reactive transport modeling. TOUGHREACT (Xu et al., 2006) is a numerical simulator that can account for non-isothermal multiphase reactive chemical transport at porous media.

2.1.3 Lumped Parameter Modelling (Tank Models)

Lumped parameter models are simplified mathematical models to simulate the behavior of geothermal reservoir fluids and forecast the future production from a field. Contrary to numerical models, lumped parameter models do not discretize the geothermal reservoir into small cells rather they represent the reservoir consisting of simple tank or combination of tanks that have individual properties. A combination of tanks can be beneficial to model a complex geothermal system as a single tank system can oversimplify the problem and cause erroneous predictions on future production.

The lumped parameter model proposed by Whiting and Ramey (1969) has successfully matched historical data and forecasted future production of Wairakei geothermal field of New Zealand. In their model, the reservoir system consisted of a single tank that has bulk volume, porosity, pressure, and temperature as parameters. The model employed a coupled model which accounts for both mass and heat balance of the system. They also proposed equations for water influx and aquifer response functions of an aquifer having infinite extent accounting different flow geometries.

Castanier et al. (1980) proposed an analytical model to simulate geothermal reservoirs, applicable to variable scenarios including all liquid, all steam, and two-phase reservoirs. Their model divides the geothermal system into three radial zones: an innermost production zone, an intermediate zone for heat transfer, and an outermost aquifer zone. The model assumes that only the innermost zone allows production. This producing zone is considered as a tank however, the pressure distribution is calculated by an analytical formulation of pressure. The intermediate zone is allowed to transfer heat and mass to the innermost zone; however, no production can occur from this zone. The temperature distribution of this zone is site specific and assumed to have a radial temperature profile. The outermost zone is assumed to be an infinite (or finite) aquifer zone. Injections to this zone is allowed in the model and leads to the flow from the outermost zone to the innermost zone. Different zone widths can be used, and if the intermediate zone width is set to zero, the model simplifies to a lumped parameter model with one tank and a recharge aquifer. This model was applied to simulate the East Mesa geothermal reservoir and compared favorably with the results of Morris and Campbell (1981), who used a three dimensional fully implicit finite difference numerical simulator.

Olsen (1984) introduced lumped parameter depletion models for liquid dominated geothermal reservoirs. These models were applied to the Svartsengi geothermal field. The study revealed that the best results with this type of model are obtained when the influx is included. The study showed that incorporating influx in the model yielded the best results. Historical production data aligned well when an infinite linear aquifer model is used with the Hurst simplified method.

Axelsson (1989) introduced a lumped parameter model consisting of series of capacitors and conductors. The capacitors represent the storage capacity of a single tank, whereas the conductors (resistors) regulate the fluid flow. The model does not account for heat balance, in other words, the temperature variations in the system were neglected. His model successfully simulated several low-enthalpy reservoirs in Iceland.

Axelsson (2005) presented successful applications of his lumped parameter model with case studies. The study revisited his 1989 paper and showed the reliability of lumped parameter models with various examples from geothermal fields around the world.

Onur et al. (2008) put forward a non-isothermal lumped-parameter model, offering a method to predict pressure and temperature behavior in liquid-dominated geothermal reservoirs. The model explained the variable rate non-isothermal flow by solving mass and energy balance equations with convection only. Their model also addresses the challenge of estimating certain reservoir parameters like bulk volume and porosity, which are hard to determine through history matching of pressure. By considering both temperature and pressure data in history matching, their model provides a way to figure out these parameters.

Hoşgör (2016) proposed a non-isothermal lumped parameter model for reservoirs containing carbon dioxide. To account for the impact of carbon dioxide on the production, the model coupled mass, heat, and carbon dioxide balances. Analytical solutions for specific cases are also presented. Sensitivity analysis on carbon dioxide reinjection is also presented.

2.2 Soil Carbon Dioxide Fluxes

Usage of soil carbon dioxide fluxes in geothermal industry mainly falls into two categories. The first is to use soil carbon dioxide flux measurements as an affordable approach in geothermal exploration. They can aid in delineating permeable structures, identifying system boundaries, estimating non-condensable gas amounts, and fine tuning the conceptual model. Second use is to measure soil fluxes to detect and quantify leaks from subsurface reservoirs during carbon capture and storage operations.

Chiodini et al. (1998) formulated the mathematical equations underpinning closed chamber soil flux measurements, subsequently implementing this methodology

across diverse volcanic and geothermal locales. Moreover, the field measurements were subjected to Sinclair's (1974) lognormal data partitioning technique, facilitating the identification of distinct populations within the soil flux measurements.

Cardellini et al. (2003) introduced a novel technique to map and quantify soil flux measurements. They applied sequential Gaussian simulations (sGs) to soil flux measurements for the first time. The study highlighted the suitability of sGs in effectively modeling soil gas fluxes while maintaining fidelity to the original data set's histogram and variogram.

CHAPTER 3

STATEMENT OF THE PROBLEM

Geothermal reservoirs in Turkey, compared to others in the world, contain significant amounts of carbon dioxide. This high level of carbon dioxide significantly impacts the performance of these reservoirs due to its effect on the flashing point and wellhead pressures. The flashing point and wellhead pressures play vital roles in the process of electricity generation at geothermal power plants. Furthermore, emission of substantial amounts of carbon dioxide into the atmosphere cause negative effects on the environment.

The goal of this study is to develop a lumped parameter model specifically for the Kızıldere Geothermal Field. This model aims to link the mass, heat, and carbon dioxide balances within the reservoir with the soil carbon dioxide data gathered at the surface. This model will be useful in the assessment of safety and feasibility of a carbon capture and storage operation. The model is useful for quantifying potential leaks from the reservoir, should they occur.

Moreover, this model can be used as a tool for tracking the carbon dioxide content of geothermal reservoirs due to its simplicity and computational efficiency compared to a full-scale numerical model. This model, requiring fewer inputs than a comprehensive numerical model, is suitable for use during initial exploration phases or as a preliminary screening tool.

CHAPTER 4

DESCRIPTION OF THE MODEL

4.1 Lumped Parameter Model

In this study, a generalized lumped parameter model that can account for soil carbon dioxide fluxes for liquid dominated geothermal systems has been developed. This model divides the geothermal system into interconnected tanks that can represent different aspects of the geothermal system. These tanks are characterized by various properties, including bulk volume (V_b), porosity (ϕ), pressure (P), temperature (T), dissolved carbon dioxide mass fraction (f_{cl}), recharge index (α), and production/reinjection rates (W_p / W_{inj}).

The generalized lumped parameter approach for modeling geothermal systems has been explored in earlier studies by researchers such as Onur et al. in 2008, Akyapı in 2011, and Hoşgör in 2016. Representation of a geothermal system by combination of tanks and solving conservation equations for tanks simultaneously is the foundation of this approach.

Individual properties of tanks can be modified to represent different components of the geothermal system, such as aquifers, heat sources, or reservoirs. There is no limit to the types and number of tanks used in a model, allowing for multiple aquifers, heat sources, or reservoir tanks. This flexibility in combining various types of tanks can significantly enhance the accuracy of field modeling. A general schematic of the proposed model can be seen in Figure 4-1.

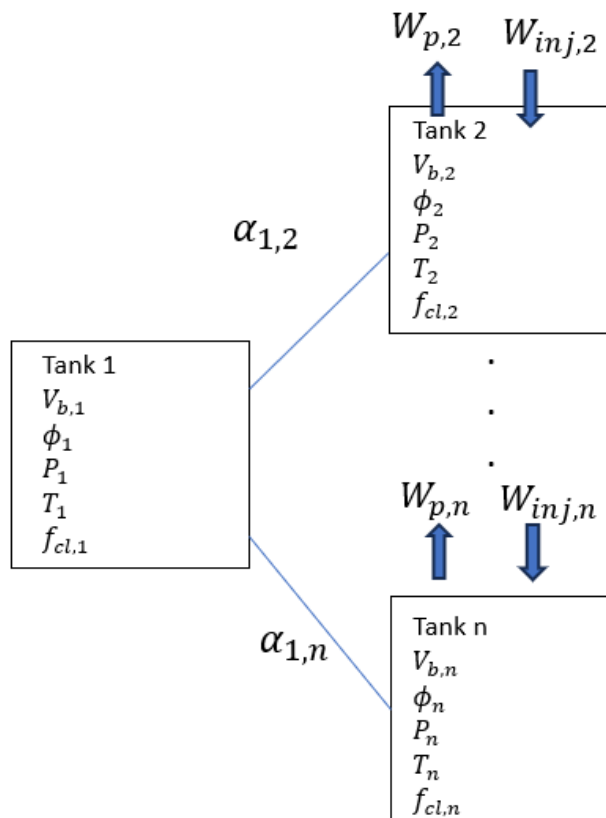


Figure 4-1 A generalized lumped parameter (tank) model comprising of n tanks of which can make $n-1$ connections.

Figure 4-1 illustrates a multi-tank model comprising n tanks. Each tank, denoted as (i) , possesses distinct property values such as bulk volume (V_b in m^3), porosity (ϕ as a fraction), pressure (P in bars), temperature (T in degrees Celsius), production rate (W_p in $kg\ s^{-1}$), reinjection rate (W_{inj} in $kg\ s^{-1}$), soil flux parameter (θ , dimensionless) and the mass fraction of dissolved carbon dioxide (f_{cl} , expressed as a fraction). Each tank has the potential to either produce, reinject, or may not be engaged in either process. A single tank has the capability to establish connections with multiple other tanks. An example model for a geothermal system can be seen in Figure 4-2.

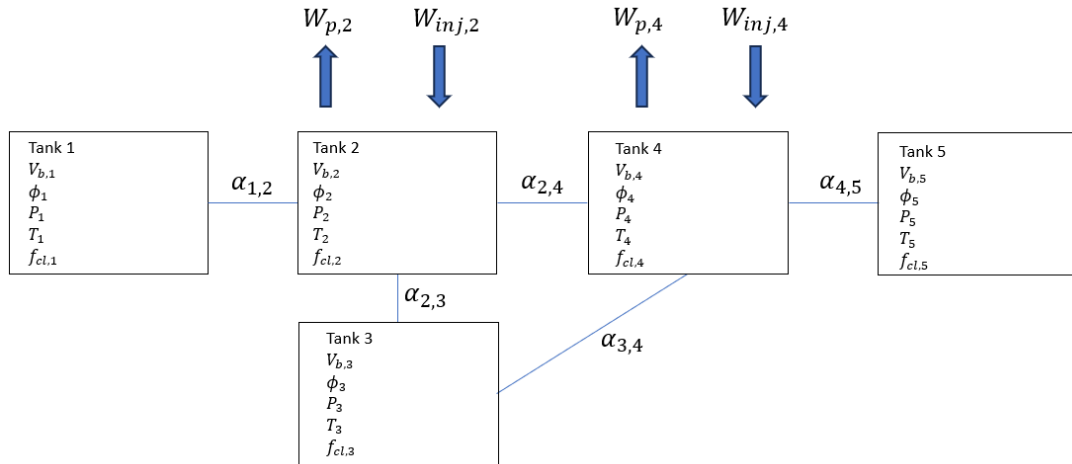


Figure 4-2 An example tank configuration for modelling a geothermal system.

The tank model depicted in Figure 4-2 features five tanks. Tanks 2 and 4 function as reservoir tanks, in which both production and reinjection occurs. Tanks 1 and 5 act as aquifers, providing pressure support to the reservoir tanks, while Tank 3 serves as a heat source. The specific parameters of each tank can be fine-tuned using historical data obtained from the reservoir. It should be noted that the example configuration shown in Figure 2 does not represent a reservoir geometry. Terms related with the reservoir geometry are lumped in recharge index (α). Figure 4-3 shows the connectivity matrix representing the configuration of the tank system for the example model.

$$C = \begin{bmatrix} 0 & \alpha_{1,2} & 0 & 0 & 0 \\ \alpha_{1,2} & 0 & \alpha_{2,3} & \alpha_{2,4} & 0 \\ 0 & \alpha_{3,2} & 0 & \alpha_{3,4} & 0 \\ 0 & \alpha_{4,2} & \alpha_{4,3} & 0 & \alpha_{4,5} \\ 0 & 0 & 0 & \alpha_{5,4} & 0 \end{bmatrix}_{5 \times 5}$$

Figure 4-3 Connectivity matrix for the given example tank configuration.

In the connectivity matrix C , the rows (denoted as i), and columns (denoted as j), represent the numbers of the respective tanks. A non-zero entry within this matrix signifies a connection between tanks i and j , whereas a zero entry indicates the

absence of a connection between tanks i and j . Additionally, this matrix stores the recharge index ($\alpha_{i,j}$) values. If tanks i and j are connected, $C(i,j)$ equals to $\alpha_{i,j}$, otherwise equals to zero.

This model incorporates conservation principles: a mass balance for the water, a mass balance for the dissolved carbon dioxide, and an overall energy balance of the system. Solving this system requires the simultaneous application of these three conservation equations to each tank at every time step. The formulation of these conservation equations is detailed in the following chapters.

4.1.1 Mass Balance for Water

Mass balance for tank i at time n can be described as follows:

$$\text{Accumulation of water at tank } i = \text{Mass rate to/from connected tanks} + \text{Net production rate from tank } i \quad (1)$$

The accumulation of water assuming a constant bulk volume (V_b) is defined as:

$$\text{Accumulation of water} = V_{b,i} \frac{d}{dt} (\rho_w \phi)_i \quad (2)$$

In equation 2, $V_{b,i}$ is the volume of the tank i (m^3), ϕ is porosity (fraction), ρ_w is the density of the liquid water (kg m^{-3}) in the tank i .

The mass rate to/from connected tanks can be calculated with the Schilthuis's (1936) steady-state flow approach:

$$\text{Mass rate to/from connected tank} \left(\frac{\text{kg}}{\text{s}} \right) = \alpha_{i,jl} (P_{jl} - P_i) \quad (3)$$

Where $\alpha_{i,j}$ is the recharge index between tanks i and j ($\text{kg bar}^{-1} \text{s}^{-1}$), P_{jl} is the pressure of the tank j_l (bars), P_i is the pressure of tank i (bars). The recharge index between tanks depicts the flow rate between tanks per pressure drop.

Given that a tank can establish connections with multiple tanks, it is necessary to sum the mass rates to/ from these interconnected tanks, hence:

$$\text{Mass rate to/from connected tanks} \left(\frac{kg}{s} \right) = \sum_{j=1}^{N_t} \alpha_{i,jl} (P_{jl} - P_i) \quad (4)$$

Where the $N_{c,i}$ is the number of connections tank i has.

The net production rate from tank i is the difference between the production rate from tank i , and the reinjection rate to tank i :

$$\text{Net production rate from tank } i = W_{p,i} + W_{inj,i} \quad (5)$$

In equation 5, $W_{p,i}$ is the production rate from tank i ($kg s^{-1}$), $W_{inj,i}$ is the reinjection rate to the tank i ($kg s^{-1}$).

Hence, the mass balance of the water at tank i can be written as Equation 6.

$$V_{b,i} \frac{d}{dt} (\rho_w \phi)_i - \sum_{n=1}^{N_t} \alpha_{i,jl} (P_j - P_i) - W_{p,i} - W_{inj,i} = 0 \quad (6)$$

4.1.2 Energy Balance

In the process of exploiting a geothermal field, water with high enthalpy is extracted from the underground reservoir, and its thermal energy is transformed into electricity. Subsequently, the effluent water, now with lower enthalpy, is reinjected back into the subsurface reservoir. As a result, monitoring the change in energy within the reservoir becomes a critical aspect of this process.

In geothermal systems, temperature variations within the reservoir are primarily caused by fluid dynamics, including production activities, flow from recharge sources, and re-injection processes. Consequently, convection typically plays a dominant role in these systems. Under these assumptions, energy balance for tank i at time n can be described as follows (Akyapi, 2011):

$$\begin{aligned} \text{Accumulation of energy at tank } i &= \text{Energy rate to/from} \\ &\text{connected tanks} \\ &+ \text{Net energy production rate} \end{aligned} \quad (7)$$

The accumulation rate of energy is defined as:

$$\frac{d}{dt} [V_b(1 - \phi)\rho_m C_m T + V_b \phi \rho_w u_w] \quad (8)$$

Where ρ_m defined as rock matrix density (kg m^{-3}), C_m defined as specific heat capacity of the rock matrix ($\text{J kg}^{-1} \text{ }^\circ\text{C}^{-1}$), u_w is specific internal energy of the water (J kg^{-1}) and T is temperature of the tank ($^\circ\text{Celsius}$).

Energy flow rate between connected tanks can be calculated as:

$$\text{Energy flow rate between connected tanks} = \sum_{j=1}^{N_t} \alpha_{i,jl} (P_j - P_i) h_y \quad (9)$$

To correctly assess the flow direction in numerical calculation an upwinding scheme for the term h_y is used as explained in (Akyapı,2011):

$$h_y = \begin{cases} h_{w,i}(T_i, t) & \text{if } p_i > p_{jl} \\ h_{w,jl}(T_{jl}, t) & \text{if } p_i < p_{jl} \end{cases}$$

Where h_w (J/kg) is the specific enthalpy of the water.

The net energy production rate from the tank can be described as:

$$\text{Net energy production rate} = W_{p,i} h_{w,i} + W_{inj,i} h_{w,inj} \quad (10)$$

Where the $h_{w,inj}$ (J kg^{-1}) is the specific enthalpy of the injection water.

Hence, the energy balance of the water at tank i can be written as Equation 11.

$$\begin{aligned} \frac{d}{dt} [V_b(1 - \phi)\rho_m C_m T + V_b \phi \rho_w u_w] - \sum_{j=1}^{N_t} \alpha_{i,jl} (P_j - P_i) h_y - W_{p,i} h_{w,i} \\ - W_{inj,i} h_{w,inj} = 0 \end{aligned} \quad (11)$$

4.1.3 Carbon Dioxide Mass Balance

Dissolved carbon dioxide mass balance for tank i at time n can be described as follows:

$$\begin{aligned} & \text{Accumulation of dissolved carbon dioxide at tank } i = \\ & \text{Dissolved carbon dioxide rate from connected tanks} + \\ & \text{Net production rate of carbon dioxide tank } i \\ & + \text{Fluxes out from this tank} \end{aligned} \quad (12)$$

The accumulation of dissolved carbon dioxide assuming a constant bulk volume (V_b) is defined as:

$$\text{Accumulation of dissolved carbon dioxide} = V_{b_i} \frac{d}{dt} (\rho_w \phi f_{cl})_i \quad (13)$$

Where $f_{cl,i}$ is the mass fraction of the dissolved carbon dioxide (fraction).

The summation of dissolved carbon dioxide mass rate to/from connected tanks given in equation 14.

$$\begin{aligned} & \text{Dissolved carbon dioxide mass rate to/from connected tank} \left(\frac{\text{kg}}{\text{s}} \right) \\ & = \sum_{j=1}^{N_t} \alpha_{i,jl} (P_j - P_i) f_{cl,y} \end{aligned} \quad (14)$$

An upwinding approach is also utilized for the dissolved carbon dioxide flows between tanks as described in Hoşgör (2016):

$$f_{cl,y} = \begin{cases} f_{cl,i} & \text{if } p_i > p_{jl} \\ f_{cl,jl} & \text{if } p_i < p_{jl} \end{cases}$$

The net production rate of dissolved carbon dioxide from tank i is the difference between the production rate of carbon dioxide from tank i , and the reinjection rate of carbon dioxide to tank i :

$$\text{Net production rate from tank } i = W_{p,i} f_{cl,i} + W_{inj,i} f_{cl,inj} \quad (15)$$

In equation 15, $f_{cl,inj}$ is the mass fraction of the dissolved carbon dioxide in the reinjection water (fraction).

Soil fluxes out from this tank can be calculated as:

$$\text{Soil fluxes out} = V_b \phi \rho f_{cl,i} \theta \quad (16)$$

Where θ is a dimensionless parameter for quantifying soil fluxes out from this tank. The main mechanism behind carbon dioxide flux from subsurface to surface is through diffusion. Therefore, the term θ should consist of a diffusion constant for the soil, a concentration gradient between the subsurface and the atmosphere, a Δz which is depth over the gradient is considered. In this study, all variables related to diffusion of carbon dioxide from subsurface to surface are collectively incorporated into the parameter θ .

Hence, the mass balance of the carbon dioxide at tank i can be written as Equation 17.

$$V_{bi} \frac{d}{dt} (\rho_w \phi f_{cl})_i - \sum_{j=1}^{N_t} \alpha_{i,jl} (P_j - P_i) f_{cl,y} - W_{p,i} f_{cl,i} - W_{inj,i} f_{cl,inj} - V_b \phi \rho f_{cl,i} \theta = 0 \quad (17)$$

4.1.4 Solution of the System of Equations

The conservation equations for mass, energy, and carbon dioxide (Equation 6, Equation 11, Equation 17) constitute a system of nonlinear equations which cannot be solved analytically. In this study, for solving the system of conservation equations, methodology described in (Onur et al., 2008; Akyapi, 2011; Hoşgör, 2016) is adopted. This methodology revolves around using Newton's method for the nonlinear set of equations. The Newton's method is defined as:

$$J^{n+1,k}(\mathbf{w}^{n+1,k}) \delta \mathbf{w}^{n+1,k+1} = -\mathbf{R}(\mathbf{w}^{n+1}) \quad (18)$$

Where, k is the iteration number. \mathbf{J} is the Jacobian matrix, \mathbf{R} is the residuals vector, $\delta\mathbf{w}$ is the difference in the solution vector between the iteration steps, and \mathbf{w} is the vector for primary variables.

Newton's method is an iterative method to find approximate solutions to nonlinear equations. The method starts with an initial guess for the solution of system at time step $n + 1$, then the guess is updated regularly using the function and the Jacobian of the system. This process continues until convergence to a predefined condition is satisfied.

To utilize Newton's method, discretized residuals for mass, energy and carbon dioxide are shown in Equation 19, Equation 20, Equation 21 respectively.

$$R_{w,i} = V_{b,i} \frac{(\rho_w \phi)^{n+1} - (\rho_w \phi)^n}{\Delta t} - \sum_{n=1}^{N_{c,i}} \alpha_{i,jl} (P_{jl} - P_i) - W_{p,i} - W_{inj,i} = 0 \quad (19)$$

$$R_{e,i} = V_{b,i} \frac{[(1 - \phi)\rho_m C_m T + \phi(\rho_w u_w)]^{n+1}}{\Delta t} - V_{b,i} \frac{[(1 - \phi)\rho_m C_m T + \phi(\rho_w u_w)]^n}{\Delta t} - \sum_{n=1}^{N_{c,i}} \alpha_{i,jl} (P_{jl} - P_i) h_y - W_{p,i} h_{w,i} - W_{inj,i} h_{w,inj} = 0 \quad (20)$$

$$R_{c,i} = V_{b,i} \frac{(\rho_w \phi f_{cl})^{n+1} - (\rho_w \phi f_{cl})^n}{\Delta t} - \sum_{n=1}^{N_{c,i}} \alpha_{i,jl} (P_{jl} - P_i) f_{cl,y} - W_{p,i} f_{cl,i} - W_{inj,i} f_{cl,inj} = 0 \quad (21)$$

The time derivatives in the equations for mass, energy, and carbon dioxide balances are discretized implicitly between time steps n , and $n + 1$ where $n + 1 = t + \Delta t$. Residuals vector can be written as:

$$\mathbf{R}^{n+1,k} = \begin{bmatrix} R_{1w} \\ R_{1e} \\ R_{1c} \\ \cdot \\ \cdot \\ R_{Ntw} \\ R_{Nte} \\ R_{Ntc} \end{bmatrix}_{3N_t}$$

Where N_t is the number of tanks in the system.

Then, the vector for primary variables, \mathbf{w} can be defined as:

$$\mathbf{w}^{n+1,k} = \begin{bmatrix} P_1^{n+1} \\ T_1^{n+1} \\ fcl_1^{n+1} \\ \cdot \\ \cdot \\ P_{N_t}^{n+1} \\ T_{N_t}^{n+1} \\ fcl_{N_t}^{n+1} \end{bmatrix}_{3N_t}$$

To solve for $\delta\mathbf{w}^{n+1,k+1}$, a Jacobian matrix that stores the first partial derivatives of the primary variables should be calculated.

$$J^{n+1,k} = \begin{bmatrix} \frac{\partial R_{1w}}{\partial P_1} & \frac{\partial R_{1w}}{\partial T_1} & \frac{\partial R_{1w}}{\partial f_{cl1}} & \cdot & \cdot & \cdot & \frac{\partial R_{1w}}{\partial P_{N_t}} & \frac{\partial R_{1w}}{\partial T_{N_t}} & \frac{\partial R_{1w}}{\partial f_{cl_{N_t}}} \\ \frac{\partial R_{1e}}{\partial P_1} & \frac{\partial R_{1e}}{\partial T_1} & \frac{\partial R_{1e}}{\partial f_{cl1}} & \cdot & \cdot & \cdot & \frac{\partial R_{1e}}{\partial P_{N_t}} & \frac{\partial R_{1e}}{\partial T_{N_t}} & \frac{\partial R_{1e}}{\partial f_{cl_{N_t}}} \\ \frac{\partial R_{1c}}{\partial P_1} & \frac{\partial R_{1c}}{\partial T_1} & \frac{\partial R_{1c}}{\partial f_{cl1}} & \cdot & \cdot & \cdot & \frac{\partial R_{1c}}{\partial P_{N_t}} & \frac{\partial R_{1c}}{\partial T_{N_t}} & \frac{\partial R_{1c}}{\partial f_{cl_{N_t}}} \\ \cdot & \cdot & \cdot & \cdot & \cdot & \cdot & \cdot & \cdot & \cdot \\ \cdot & \cdot & \cdot & \cdot & \cdot & \cdot & \cdot & \cdot & \cdot \\ \frac{\partial R_{Ntw}}{\partial P_1} & \frac{\partial R_{Ntw}}{\partial T_1} & \frac{\partial R_{Ntw}}{\partial f_{cl1}} & \cdot & \cdot & \cdot & \frac{\partial R_{Ntw}}{\partial P_{N_t}} & \frac{\partial R_{Ntw}}{\partial T_{N_t}} & \frac{\partial R_{Ntw}}{\partial f_{cl_{N_t}}} \\ \frac{\partial R_{Nte}}{\partial P_1} & \frac{\partial R_{Nte}}{\partial T_1} & \frac{\partial R_{Nte}}{\partial f_{cl1}} & \cdot & \cdot & \cdot & \frac{\partial R_{Nte}}{\partial P_{N_t}} & \frac{\partial R_{Nte}}{\partial T_{N_t}} & \frac{\partial R_{Nte}}{\partial f_{cl_{N_t}}} \\ \frac{\partial R_{Ntc}}{\partial P_1} & \frac{\partial R_{Ntc}}{\partial T_1} & \frac{\partial R_{Ntc}}{\partial f_{cl1}} & \cdot & \cdot & \cdot & \frac{\partial R_{Ntc}}{\partial P_{N_t}} & \frac{\partial R_{Ntc}}{\partial T_{N_t}} & \frac{\partial R_{Ntc}}{\partial f_{cl_{N_t}}} \end{bmatrix}_{3N_t \times 3N_t}$$

Jacobian matrix stores the partial derivatives and reflects how the system behaves given the change of primary variables.

The update of the solution vector is done as follows:

$$J^{n+1,k}(\mathbf{w}^{n+1,k})\delta\mathbf{w}^{n+1,k+1} = -\mathbf{R}(\mathbf{w}^{n+1})$$

$$\mathbf{w}^{n+1,k+1} = \mathbf{w}^{n+1,k} + \delta\mathbf{w}^{n+1,k+1}$$

The difference in the solution vector is calculated for the current iteration, then a convergence check is applied. Convergence criterion for this system is selected to be $\delta\mathbf{w} < 10^{-8}$. This threshold ensures that the solution has reached a sufficient level of precision. The flow chart for the solution of the system of equations is given in Figure 4.

To improve the robustness of the method, a backtracking applied at each convergence check step. This backtracking involves adapting the step size taken each iteration to ensure that the successive approximations are moving towards a root.

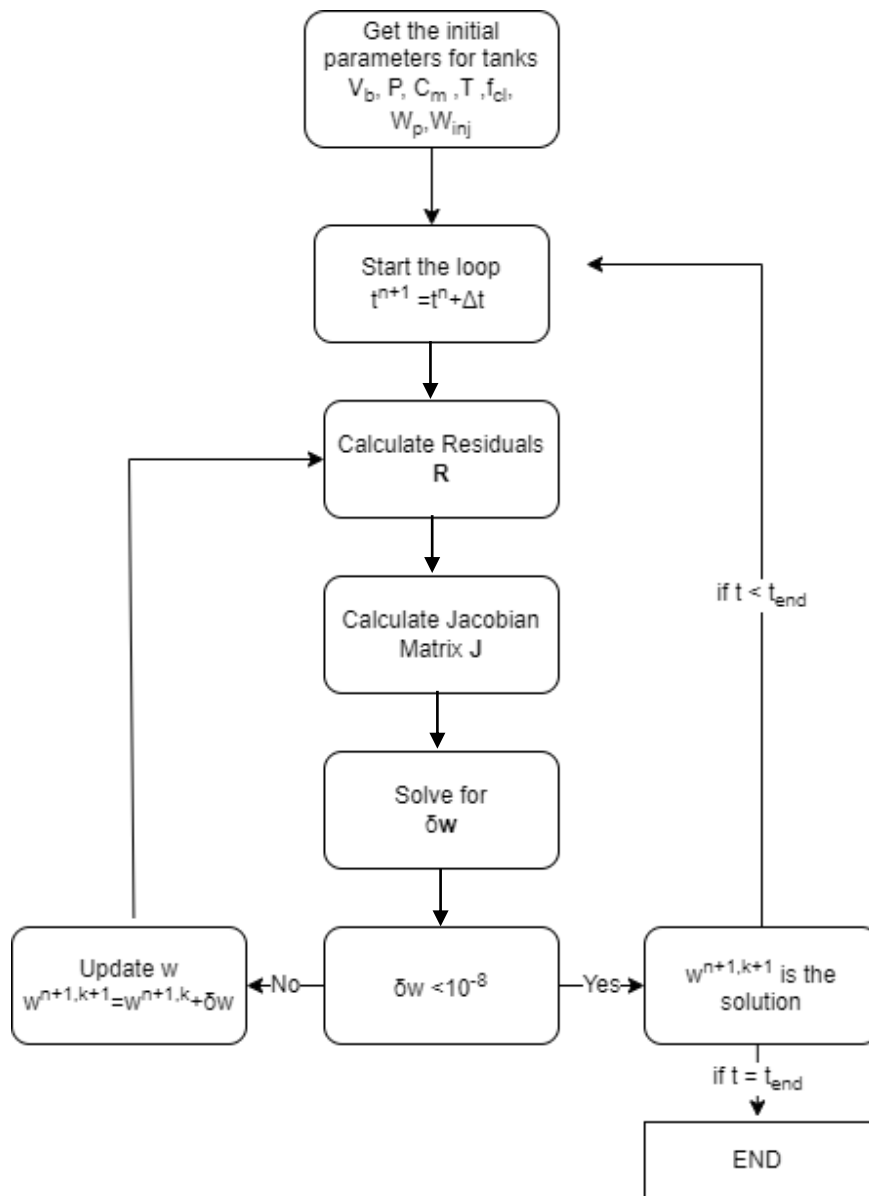


Figure 4-4 Flow chart of the solution algorithm.

4.1.5 Validation of the Model

The generalized tank model developed in this study is compared with the analytical model developed by Hoşgör (2016) for validation purposes. In Hoşgör's work (2016), a new analytical model is introduced to estimate dissolved carbon dioxide levels over time in liquid-dominated geothermal reservoirs, based on production,

reinjection, and recharge rates. The model operates on the principle of mass balance applied to carbon dioxide within a defined tank volume. This conceptual tank is characterized by its bulk volume (V_b), porosity (ϕ), and the initial carbon dioxide mass fraction in the reservoir (f_0). The model also assumes that the tank is filled with water at a specific density (ρ). The ordinary differential equation, derived from the application of mass balance principles to the conceptual tank, is then solved using analytical methods. This approach provides a systematic way to analyze and predict carbon dioxide behavior in liquid dominated geothermal reservoirs. The analytical expression derived for constant mass fraction of injected carbon dioxide is given in equation 22.

$$f(t) = f_0 e^{-\left(\frac{W_p c_t}{\kappa} t\right)} + \frac{W_{inj} f_{inj} + W_n f_{re}}{W_p} + \frac{W_n f_{re}}{W_p - \frac{\alpha}{c_t}} e^{-\left(\frac{W_p c_t}{\kappa} t\right)} - \frac{W_n f_{re}}{W_p - \frac{\alpha}{c_t}} e^{-\left(\frac{\alpha}{\kappa} t\right)} \quad (22)$$

Where f_0 is the initial carbon dioxide mass fraction (fraction), W_p is the production rate (kg s^{-1}), W_{inj} is the injection rate (kg s^{-1}), W_n is the net drawdown from reservoir (kg s^{-1}), f_{re} is the carbon dioxide mass fraction of recharge source (fraction), α is the recharge index ($\text{kg bar}^{-1} \text{ s}^{-1}$), c_t is the total compressibility (bar^{-1}), κ is the storage capacity (kg bar^{-1}), t is the time (seconds).

Equation 22 gives the carbon dioxide mass fraction with respect to time for a liquid dominated reservoir. This analytical solution is obtained for cases where the reinjection carbon dioxide mass fraction is kept constant. This analytical solution is used to validate the developed lumped parameter model. A synthetic scenario is simulated by both the lumped parameter model developed and the analytical solution given in Equation 22. The constructed hypothetical scenario involves a reservoir with an initial pressure of 130 bars, an initial temperature of 200 degrees Celsius, and an initial dissolved carbon dioxide concentration of 0.021. The parameters used in the lumped parameter model and the analytical solution are given in tables 4-1,4-2 respectively.

Table 4-1 Parameters used in lumped parameter model.

Bulk Volume of the reservoir tank, m ³	31.5x10 ⁹
Bulk Volume of the recharge tank, m ³	10 ⁵⁰
Porosity of the reservoir tank, fraction	0.05
Porosity of the recharge tank, fraction	0.05
Recharge index, kg bar ⁻¹	243.5
Production rate, kg s ⁻¹	2000
Injection Rate, kg s ⁻¹	1900
Total compressibility, bar ⁻¹	1x10 ⁻⁴
Reinjection carbon dioxide mass fraction, fraction	0
Initial carbon dioxide mass fraction, fraction	0.021

Table 4-2 Parameters used in analytical solution.

Bulk Volume, m ³	31.5x10 ⁹
Porosity, fraction	0.05
Total compressibility, bar ⁻¹	1x10 ⁻⁴
Recharge index, kg bar ⁻¹	40
Production rate, kg s ⁻¹	2000
Injection Rate, kg s ⁻¹	1900
Total compressibility, bar ⁻¹	1x10 ⁻⁴
Reinjection carbon dioxide mass fraction, fraction	0
Initial carbon dioxide mass fraction, fraction	0.021

To simulate a recharge source in the lumped parameter model, a tank having higher bulk volume (10^{50} m^3) and same initial properties with the reservoir tank is used. The porosity of both recharge tank and the reservoir tank is given same. The comparison of lumped parameter model and the analytical solution is given in Figure 4-5.

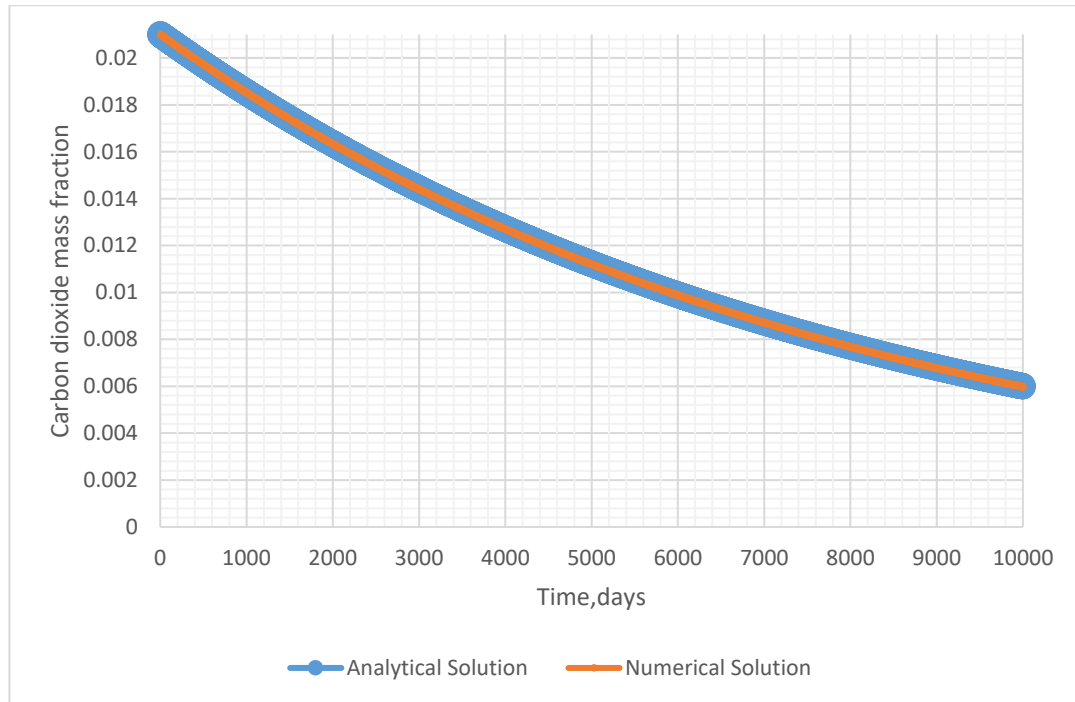


Figure 4-5 Comparison of Analytical and Numerical Solution

The carbon dioxide mass fractions, as calculated by both the lumped parameter model and the analytical solutions, display a remarkable agreement. In both models, the carbon dioxide content in the reservoir decreases exponentially, attributed mainly to the reinjection of water with zero dissolved carbon dioxide. Despite some carbon dioxide recharging from the recharge tank, production-reinjection rates dominate, and lead to a dilution of carbon dioxide levels in the reservoir.

4.2 Soil Carbon Dioxide Fluxes

Soil carbon dioxide flux refers to the rate at which carbon dioxide is transferred from the soil into the free air. The source of carbon dioxide moving from soil to the atmosphere can be attributed to various factors, such as plants, microorganisms, or underlying geothermal or volcanic activities. Within the framework of the GECCO project at Kızıldereli, soil flux measurements were carried out using the LI-COR LI8100A automated system (LI-COR, 2015), designed specifically for monitoring soil carbon dioxide flux. LI8100A system estimates the rate at which the soil carbon dioxide diffuses into the atmosphere by using a closed accumulation chamber (Madsen et al, 2009). In closed chamber measurements, a small sample of air is cycled from a chamber to an infrared gas analyzer (IRGA) and then returned to the chamber. The carbon dioxide flux (F_c) is calculated using Equation 23, which considers various parameters including the volume of the chamber, the area of the soil surface, air temperature, atmospheric pressure, and the rate of CO₂ concentration increase within the chamber.

$$F_c = \frac{PV}{RTS} \frac{\partial C_c}{\partial t} \quad (23)$$

Where, F_c is the soil carbon dioxide rate ($\mu\text{mol m}^{-2} \text{s}^{-1}$), R is the gas constant, V (cm^3) is the volume, P is the atmospheric pressure (Pa), S is soil area encompassed by the chamber (m^2), T is absolute temperature ($^\circ\text{K}$), and $\frac{\partial C_c}{\partial t}$ is the rate of change of carbon dioxide mole fraction ($\mu\text{mol mol}^{-1}$) (Madsen et al., 2009).

The rate of carbon dioxide concentration increase within the chamber is calculated by exponentially fitting the concentration over time. After determining the rate of carbon dioxide concentration increase, carbon dioxide flux can be calculated. For accurate soil flux readings, it's important to omit some initial data points that are affected by external factors like the movement of the chamber from fitting process. This exclusion period is known as the "dead band." For the soil flux measurements conducted in Kızıldereli, the dead band period has been established as 20 seconds.

SoilFluxPro computer program by LI-COR Biosciences (LI-COR,2021) is used for fitting process.

For field measurements, PVC soil collars, which accommodate the accumulation chamber, are installed one day prior to the measurements. This preparation is done to minimize disturbances resulting from the installation process. The duration for each measurement is set at 90 seconds, and at each point, two measurements are taken. Additionally, soil temperature and relative humidity are recorded, given their significant impact on soil fluxes.

CHAPTER 5

MODELLING CARBON DIOXIDE CONTENT OF KIZILDERE GEOTHERMAL FIELD

In this chapter, application of the developed lumped parameter to the pilot carbon dioxide reinjection at Kızıldere Geothermal Field is described.

Geothermal fields in the Western part of Turkey are known for their significant carbon dioxide content that results in considerably high amounts of gas emissions from geothermal power plants during electricity production. Geothermal Emission Control (GECO) project aims to address this issue and minimize the amount of carbon dioxide emitted on the fields with similar characteristics around Europe. In the framework of GECO project, the emitted carbon dioxide is reinjected into the reservoir as a method of reducing carbon dioxide emissions to the atmosphere similar to the CarbFix method carried out in Iceland. One of the pilot reinjection schemes was set up in the Kızıldere geothermal field in Turkey.

As part of the GECO project, a portion of the carbon dioxide produced at the Kızıldere Geothermal Field has been reinjected back into the geothermal reservoir. For this pilot carbon dioxide reinjection, a specific well within the field was chosen for the task. Following evaluations of observability, cost-effectiveness, and the aim to minimize commercial risks, well KD50A was selected as the appropriate well for reinjecting the carbon dioxide back into the reservoir (Senturk, Taylan Akin 2021).

The proposed carbon dioxide reinjection design can be seen in Figure 5-1. Approximately 0.3% weight of carbon dioxide is reinjected into the reservoir, between October 2022, and March 2023. The system for reinjection is designed to guarantee that the carbon dioxide is fully dissolved in brine.

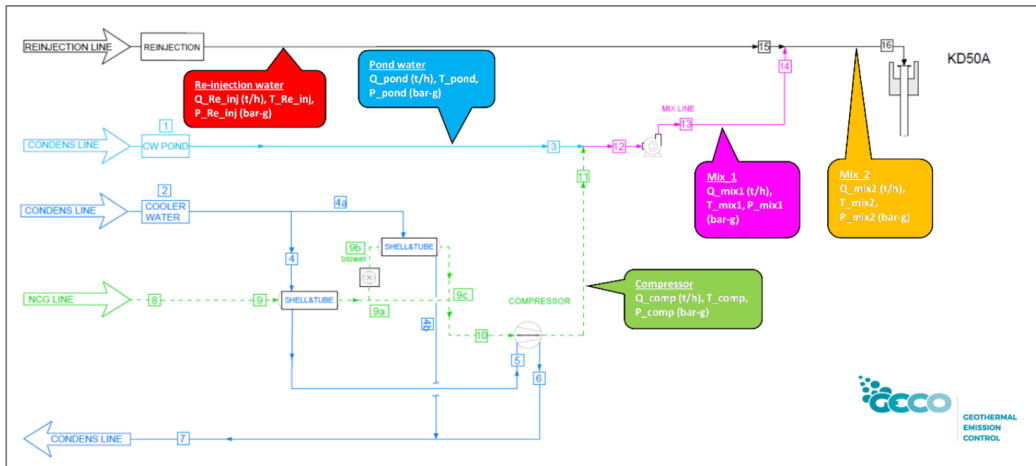


Figure 5-1 Carbon dioxide reinjection design for well KD50A (Akın et al., 2023)

In this reinjection scheme, carbon dioxide at approximately 85 °C is collected from the exhaust at the power plant's cooling tower and directed to a compressor system. The pressurized carbon dioxide is then mixed with bypass pond, at pressures ranging between 12 to 14 bar-g. This carbon dioxide-enriched mixture is then pressurized to 34 bar-g by a booster pump. This pressurization is required to transport the mixture to the reinjection wellhead, where it is mixed with the reinjection brine. The resultant mixture, at the KD-50A wellhead, is then injected into the reservoir. Logging units are installed at various steps to monitor fluid properties to make sure that carbon dioxide is fully dissolved in brine.

5.1 Study Area

Located in Denizli, in Turkey's western region, the Kızıldere Geothermal Field is recognized as the country's largest and most crucial geothermal site. It was discovered in 1965 by the General Directorate of Mineral Research and Exploration of Turkey (MTA). Following this discovery, a pilot power plant with a capacity of 500 kWe was commissioned in 1974. The field, featuring a power plant of 17.4 MWe, remained under the operation of the state-owned Electricity Generation Corporation (EÜAŞ) until 2008. On September 1, 2008, the Zorlu Group acquired the exploitation license for the Kızıldere Geothermal field, along with the existing

Power Plant (Kızıldere-I), through a privatization tender (Kaya & Kindap 2009). After obtaining the exploitation license, Zorlu Energy initiated the development of two additional power plants: Kızıldere II (80 MWe), which commenced in 2013, and Kızıldere III (165 MWe), with Phase 1 starting in 2017 and Phase 2 in 2018 (Şentürk, 2021).

Geological, geophysical, and geochemical studies, which were supported by United Nations Development Program, showed the existence of two distinct reservoir levels: a shallow medium enthalpy layer and a deep high enthalpy layer (Gokcen et al., 2004). The deeper reservoir, which is composed of metamorphic rocks, typically contains 3% carbon dioxide by weight, while the shallower reservoir section generally contains 1.5% carbon dioxide by weight (Şimşek et al., 2005).

The Kızıldere geothermal field is located in the western region of Turkey, an area notable for its horst and graben geological structures, positioned between the Buldan and Babadağ horsts. This field lies in close proximity to the serpentine path of the Büyük Menderes River. Figure 5-2 provides a visual representation of the conceptual model of the geothermal system, as well as an overview of the general geological context of the area.

The Sazak reservoir formation, which is shallower, is overlain by the impermeable Kolonkaya formation, while the second reservoir zone is covered by the Kızılburun formation. The high enthalpy of this system is attributed to a source located approximately 9 kms under surface, and the deep circulation of meteoric waters. Water precipitated in the surrounding aquifers is heated at increasing depths and moves along the faults and the fracture zones to recharge the reservoir. Surface manifestations of the underlying geothermal system such as fumaroles and thermal springs are also present at Kızıldere geothermal field.

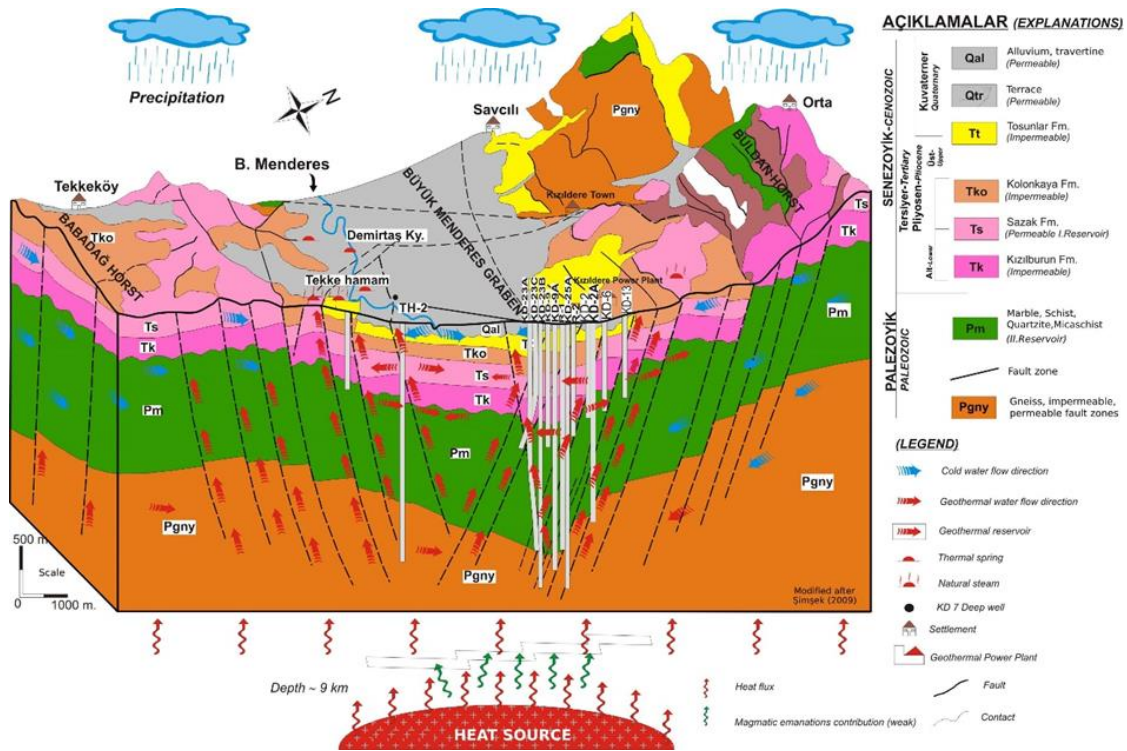


Figure 5-2 Detailed conceptual model of Kızıldere Geothermal Field and geological setting (modified as per the adaptations from Şimşek et al., 2009).

5.2 Lumped Parameter Modelling

Using the developed lumped parameter model in this study, a sector model of the Kızıldere Geothermal Field for the pilot carbon dioxide reinjection is created. This sector model encompasses the pilot reinjection well KD50A and its surrounding area. The coverage of the sector model can be seen in Figure 5-3.

For the lumped parameter model, a two-tank approach is considered. The first tank represents the recharge to the second tank, and the second tank represents the sector model area. This tank configuration is illustrated in Figure 5-4.

In this study, it is assumed that both tanks are in equilibrium initially, in other words, the initial pressures and temperatures are assumed to be same for both tanks.

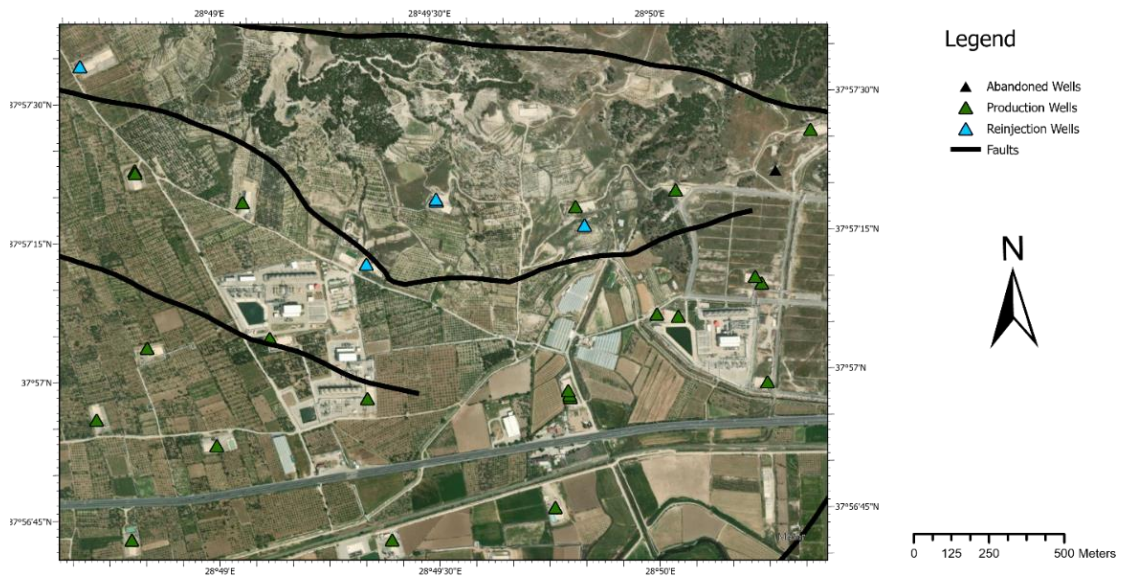


Figure 5-3 Area covered by the sector model for the Kızıldere Geothermal Field.

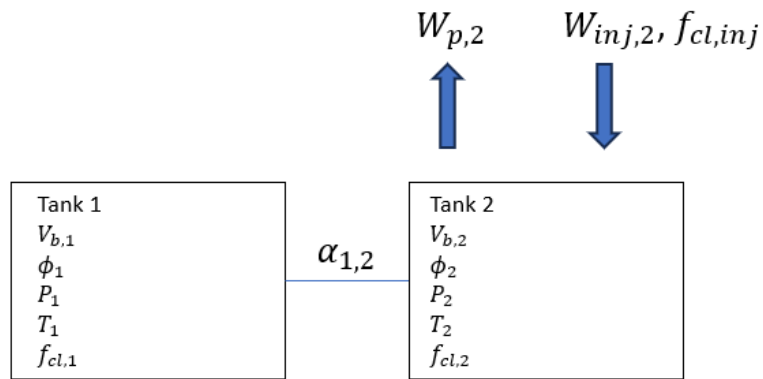


Figure 5-4 The two-tank configuration for the sector model.

The sector model consists of 4 reinjection wells, and 14 production wells. For being able to make successful predictions, the model should be history matched using the historical data of the Kızıldere Geothermal Field. The total production-reinjection history of the wells in sector model area between September 1st 2013 and June 1st, 2023, is given in Figure 5-5.

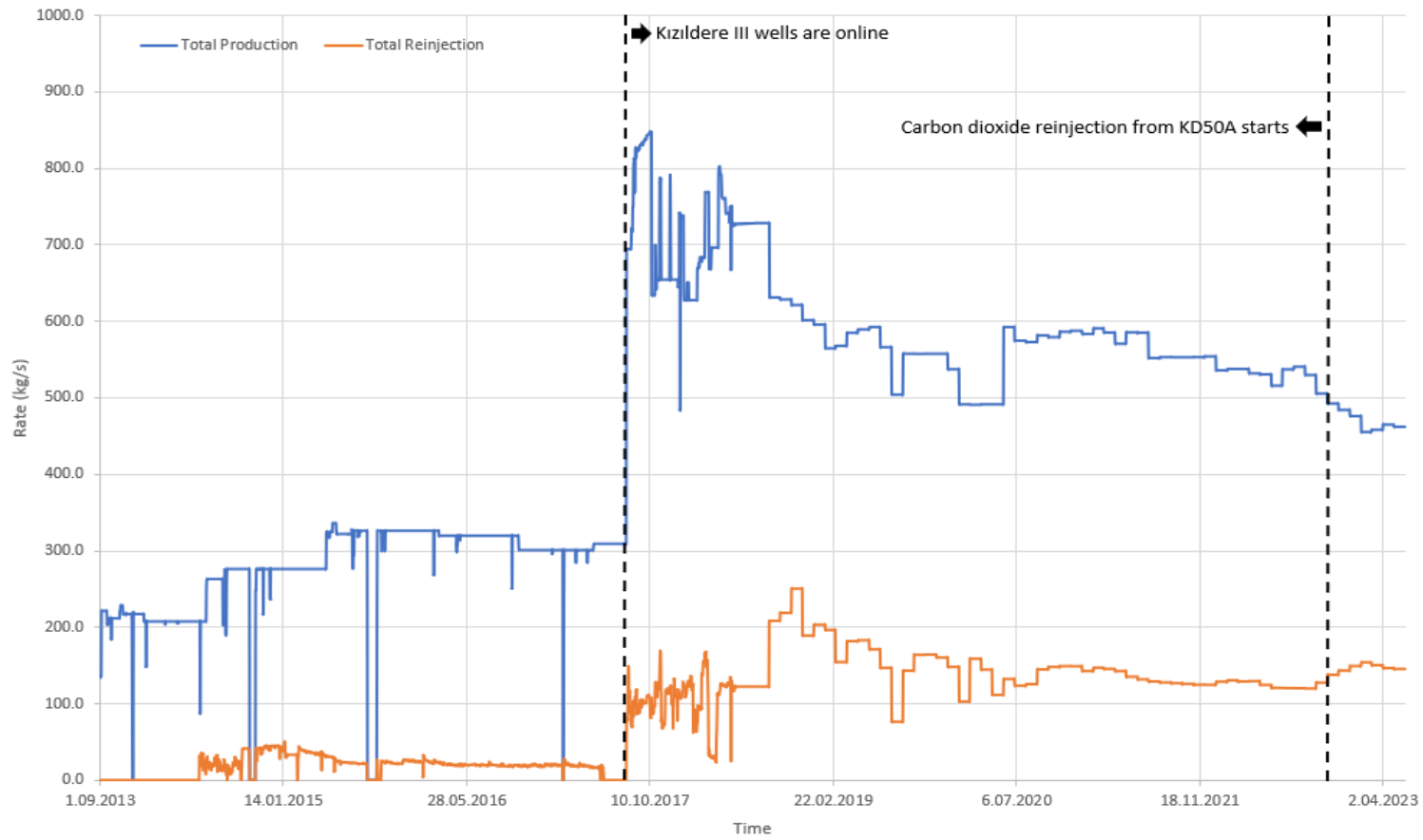


Figure 5-5 Total production-reinjection history of sector model area.

The start date for the model is set as September 1st, 2013, coinciding with the commencement of the Kızıldere II Power Plant, as some of the wells in the sector model were part of this phase of the Kızıldere project. As illustrated in Figure #, there is an observable increase in total productions and reinjections subsequent to the activation of the wells from Kızıldere III Power Plant Phase I (2017), and Kızıldere III Phase II (2018).

The two-tank model designed for the Kızıldere Geothermal Field is history matched using both static and observational pressure measurements from well KD50A. Prior to the launch of the Kızıldere III power plant in 2018, well KD50A served as an observation well from August 9, 2015, to August 2, 2016. Additionally, on May 15, 2014, the operating company conducted a static temperature and pressure measurement at the KD50A well. In this study, the pressure response observed in well KD50A is assumed to reflect the pressure conditions of the reservoir tank (Tank 2 in Figure 5-4) represented in the model. Consequently, the two-tank model is calibrated using the aforementioned static and observational data. The outcomes of this calibration are displayed in Figure 5-6.

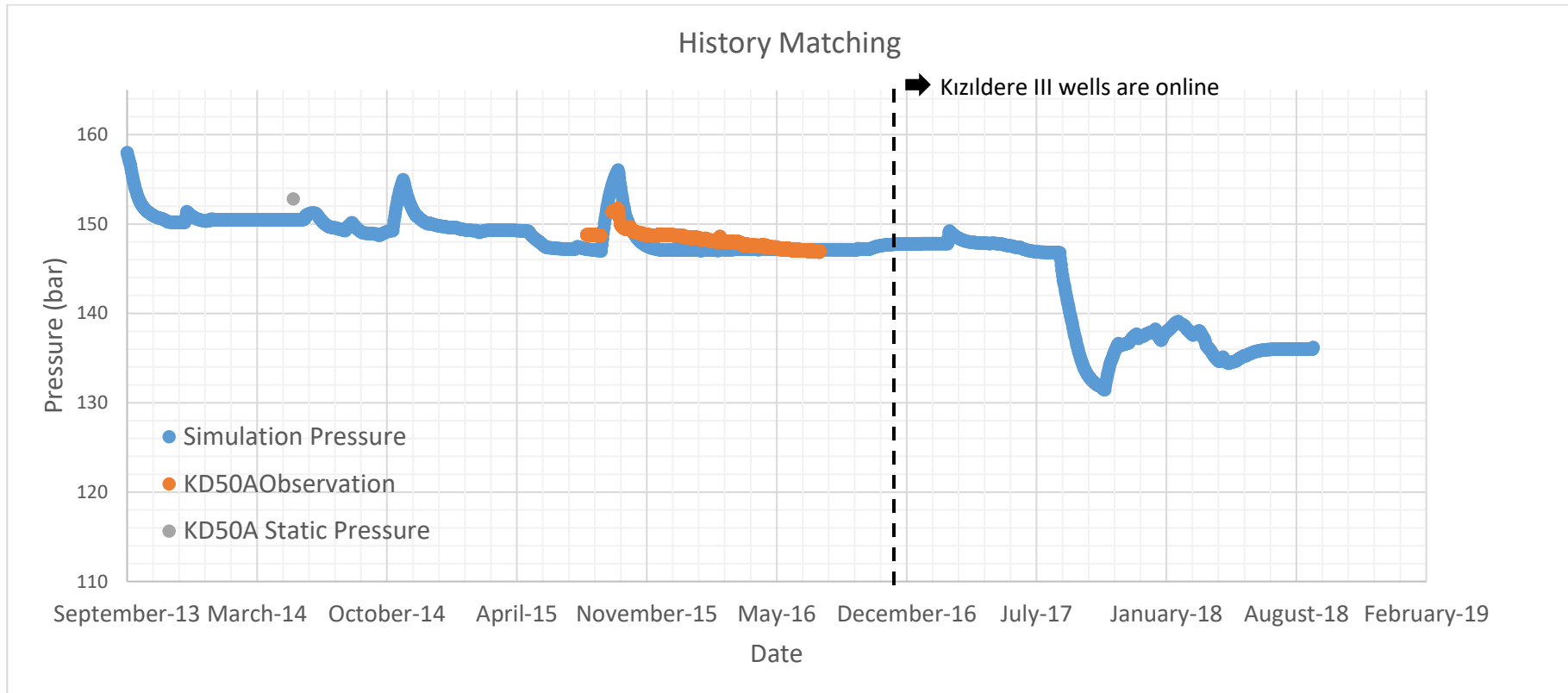


Figure 5-6 Simulated and Observed Pressures for the reservoir tank.

Figure 5-6 shows the good agreement between the simulated pressures for the reservoir tank and the observed pressures from well KD50A. The observed pressure increase at well KD50A between 28.08.2015 and 26.10.2015 is linked to a reduction in net production during this timeframe. This pressure rise is also accurately replicated by the simulation, confirming model's capability to effectively mimic the pressure dynamics of the study area. The response to a change in the system differs slightly between observation and simulated pressures. At 24.09.2015, the observed pressure at the KD50A well is 151.5 bars, whereas in the lumped parameter model 155.1 bars. This difference can be attributed to sector model having lower bulk volume compared to the rest of the reservoir.

The dissolved carbon dioxide mass fraction in the reservoir is determined by flow averaging of carbon dioxide mass fractions from wells at the reservoir level, as outlined in Equation 24. This process involves calculating the average based on the flow rates and carbon dioxide concentrations from various wells, providing a representative initial value for the carbon dioxide content in the reservoir. The carbon dioxide mass fractions at the reservoir level for wells of interest are provided by Zorlu Energy. The comparison of simulated and flow averaged carbon dioxide fractions can be seen in Figure 5-7.

$$f_{cl} = \sum_{k=1}^{wn} \left(\frac{W_p(k)}{W_{p,total}} \right) f_{cl}(k) \quad (24)$$

Where k is the number of production wells in the system, wn is the total number of wells in the sector model area, $W_p(k)$ refers to production rate of well k (kg s^{-1}), and $f_{cl}(k)$ is the dissolved carbon dioxide fraction at reservoir, fraction.

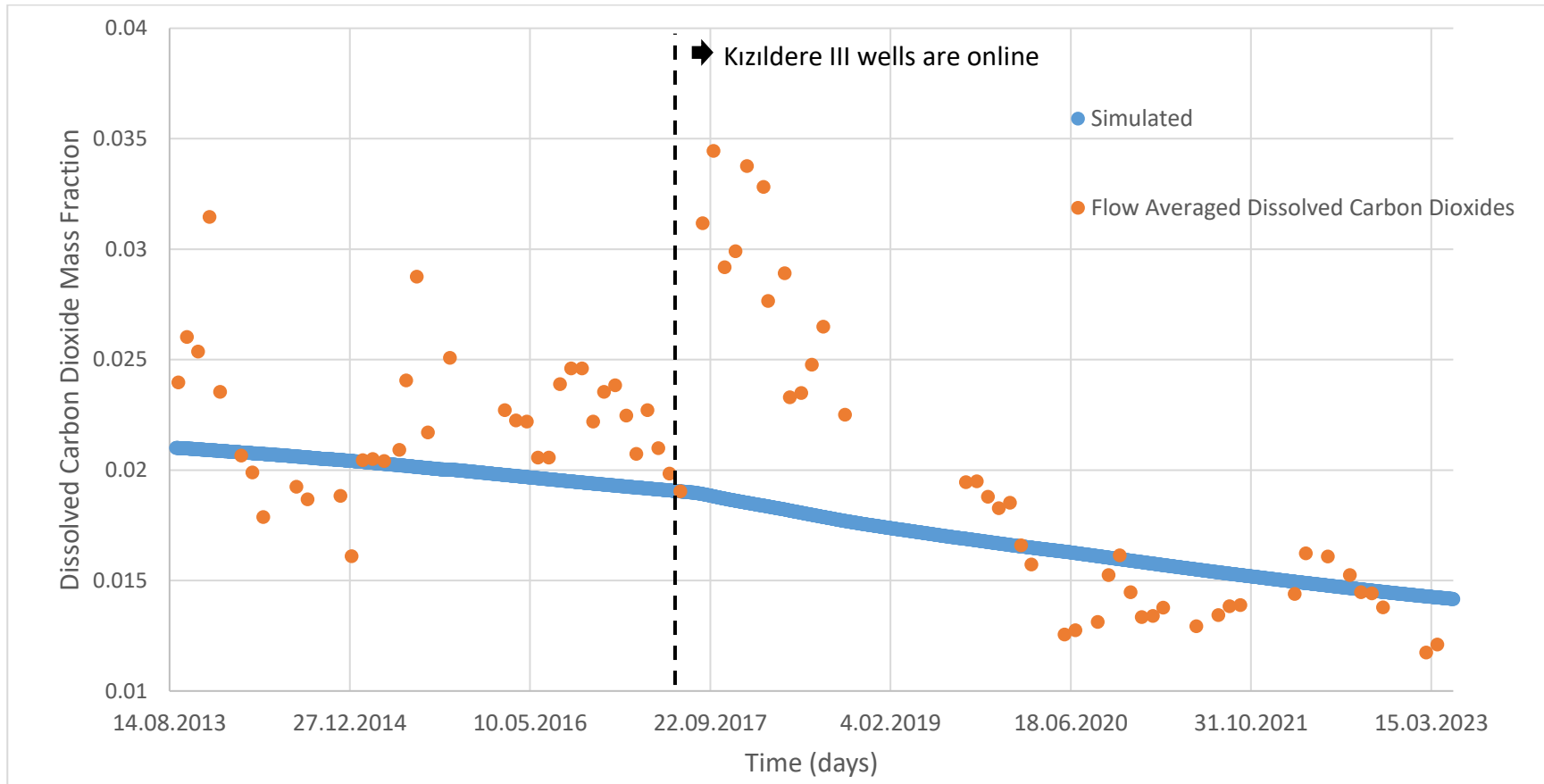


Figure 5-7 Simulated and flow averaged dissolved carbon dioxides.

Figure 5-7 shows how lumped parameter model compares with the historical carbon dioxide fractions of the study area. While the primary expected pattern for the dissolved carbon dioxide fraction in the reservoir is an exponential decline, some anomalies in the historical data from September 2017 to August 2018 deviate from this trend. These deviations are explained by the method used to calculate flow averaged carbon dioxide fractions. The flow averaged carbon dioxide fractions are calculated from the wells that are operational at the specified time. With the commencement of operation at Kızıldere III wells, which contain higher dissolved carbon dioxide fractions compared to Kızıldere II wells, flow averaged carbon dioxide fractions increase temporarily. Consequently, in the process of history matching, values that are significantly affected by the addition of these new wells with higher carbon dioxide levels are excluded from the process.

For tuning the parameter of soil fluxes, θ , August 2022 and March 2023 soil carbon dioxide flux measurements are utilized. Both measurements are conducted by the methodology of soil flux measurements described in Chapter 3. Locations of the August 2022 measurements are given in Figure 5-8.

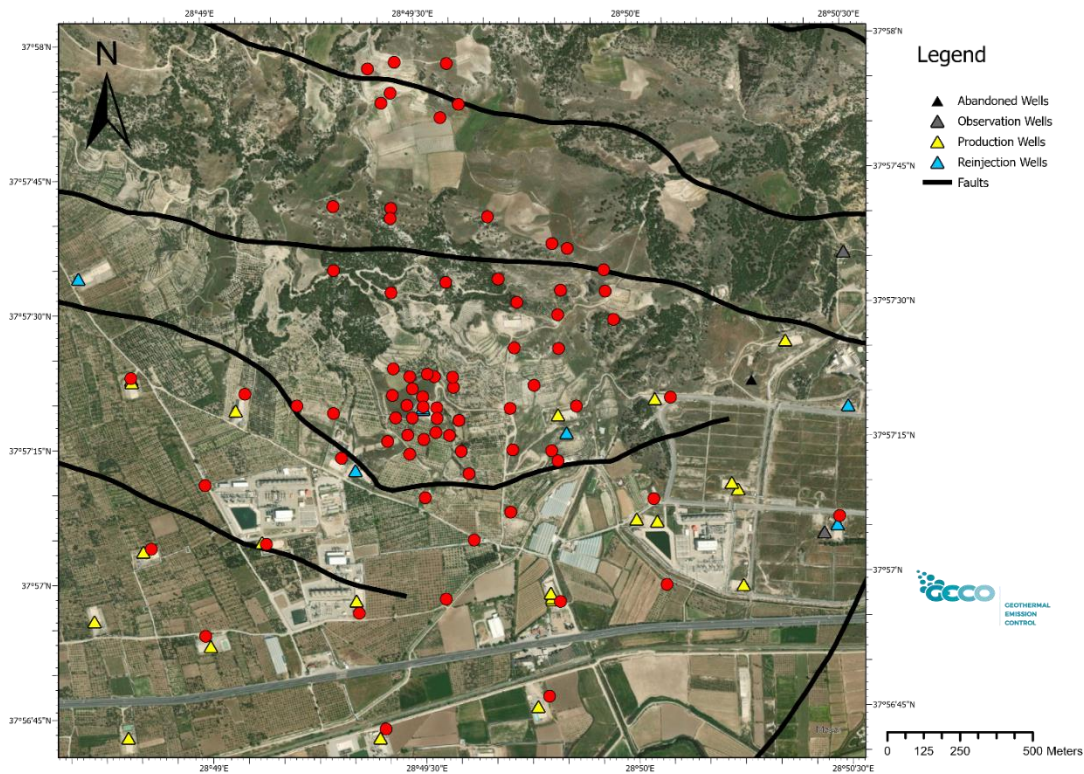


Figure 5-8 August 2022 measurement locations, wells, and faults.

A total of 79 carbon dioxide measurements were performed in August 2022 on dry soil with stable atmospheric conditions to eliminate external effects on the soil flux measurements. The soil carbon dioxide fluxes in 2022 August measurements ranged from $0.7 \text{ g m}^{-2} \text{ d}^{-1}$ to $88.8 \text{ g m}^{-2} \text{ d}^{-1}$ with a standard deviation of $11.8 \text{ g m}^{-2} \text{ d}^{-1}$. Descriptive statistic of the August 2022 measurements can be seen in Table 5-1 and individual flux results can be observed in Figure 5-9.

Table 5-1 Descriptive statistics for the August 2022 soil carbon dioxide flux measurements conducted at Kızıldereli.

Minimum ($\text{g m}^{-2}\text{d}^{-1}$)	1 st quartile ($\text{g m}^{-2}\text{d}^{-1}$)	Median ($\text{g m}^{-2}\text{d}^{-1}$)	Mean ($\text{g m}^{-2}\text{d}^{-1}$)	3 rd quartile ($\text{g m}^{-2}\text{d}^{-1}$)	Max ($\text{g m}^{-2}\text{d}^{-1}$)
0.70	3.20	5.53	8.86	9.67	88.78

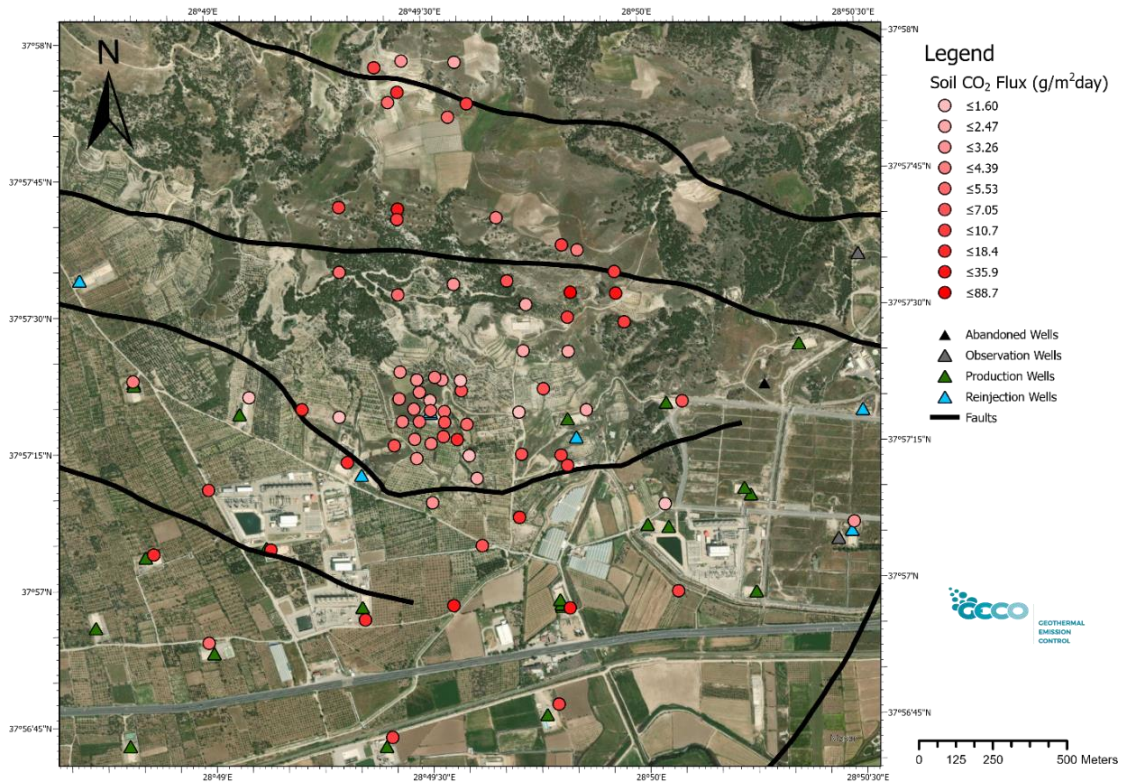


Figure 5-9 August 2022 point-based soil carbon dioxide flux results

There is noticeable variation in soil flux values, which can be attributed to differences in soil characteristics across various areas. This variation may be due to natural factors or agricultural practices common around the Kızıldere field. Studies, such as those by Altıkat et al. (2019), have shown that using farmyard manure can increase soil carbon dioxide fluxes. Additionally, variations in the geological features at the surface, like fault outcrops, contribute to this variation. Higher flux values are often found near fault outcrops, as indicated by black lines in Figure 5-9.

To examine the distribution of the sample population, a plot of cumulative probabilities against the logarithm of the soil flux measurements from August 2022 is created. This approach is based on the general observation that soil flux measurements typically exhibit lognormal characteristics.

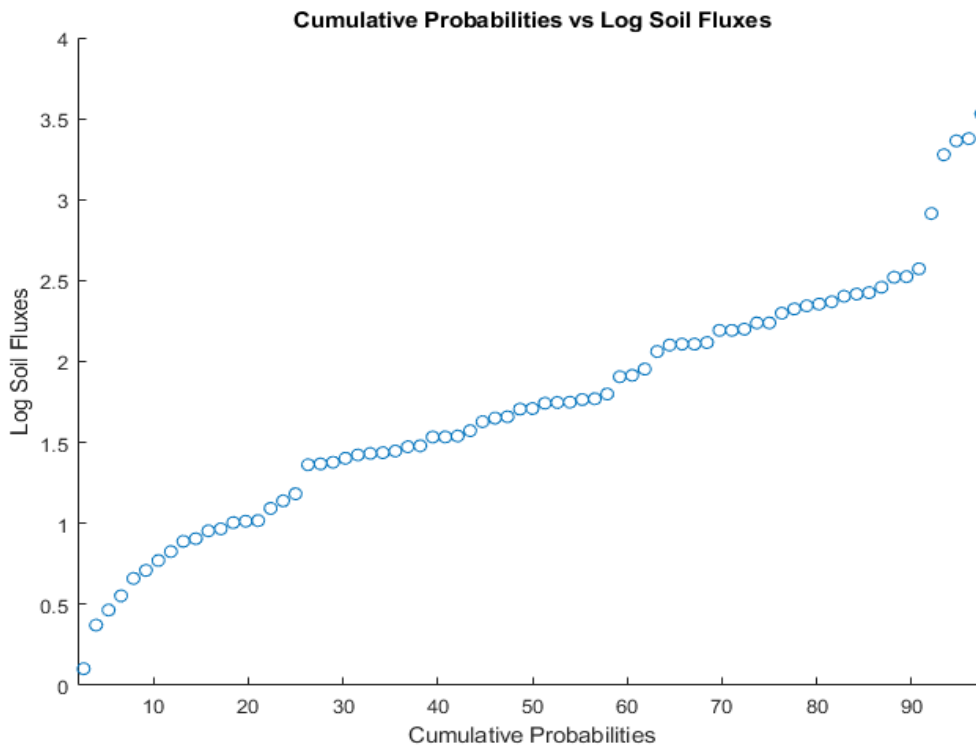


Figure 5-10 Cumulative Probabilities vs logarithm fluxes of the August 2022 soil flux measurements

The distribution of the soil flux samples corresponds to a bi-modal lognormal distribution characterized by inflections points (Figure 5-10), which is common in most geothermal and volcanic areas (Chiodini et al., 1996,1998; Sbrana et al., 2021). This phenomenon can be attributed to the fact that the measurements obtained are a composite of fluxes emanating from biogenic processes and those arising from Earth’s degassing (Camarda et al., 2019), consequently, resulting in a combination of lognormal populations.

The same analytical procedures used for the August 2022 soil flux measurements are also applied to those taken in March 2023. In March, soil flux measurements are gathered from the same locations as in August 2022. However, due to unsuitable weather conditions, it was not feasible to measure at some points. In March 2023, five months after the start of carbon dioxide reinjection, in total 66 soil carbon dioxide measurements were conducted. The soil carbon dioxide fluxes ranged from

1.84 g m⁻² d⁻¹ to 31.89 g m⁻² d⁻¹ with a mean soil flux of 9.78 g m⁻² d⁻¹. Descriptive statistics of the March 2023 measurements can be seen in Table 5-2.

Table 5-2 Descriptive statistics of the March 2023 soil carbon dioxide flux measurements at Kızıldere.

Minimum (g m ⁻² d ⁻¹)	1 st quartile (g m ⁻² d ⁻¹)	Median (g m ⁻² d ⁻¹)	Mean (g m ⁻² d ⁻¹)	3 rd quartile (g m ⁻² d ⁻¹)	Max (g m ⁻² d ⁻¹)
1.84	4.77	8	9.78	12.61	31.89

The standard deviation of the data set is 7.1 g m⁻² d⁻¹. Similar to the pre reinjection results, this high variance in the data set can be explained by spatial variation of the soil properties and geological features across the field. August 2022 Individual soil flux results at locations can be seen in Figure 5-11.

Like the results observed prior to reinjection, relatively higher flux values are observed near fault outcrops.

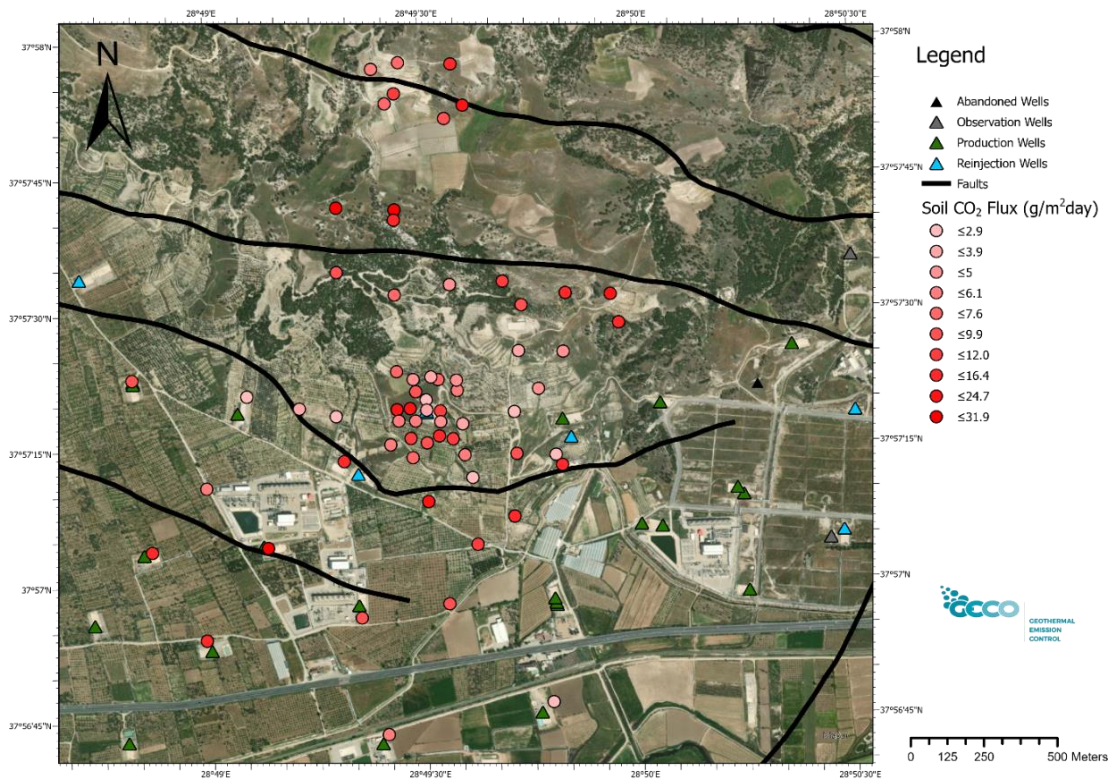


Figure 5-11 Soil carbon dioxide flux results of March 2023 measurements.

To determine the distribution of soil flux measurements, cumulative probabilities versus logarithms of soil flux measurements are plotted in Figure 5-12.

Figure 5-12 implies that March 2023 results show lognormal bimodal distribution since the plot is nonlinear with inflection points.

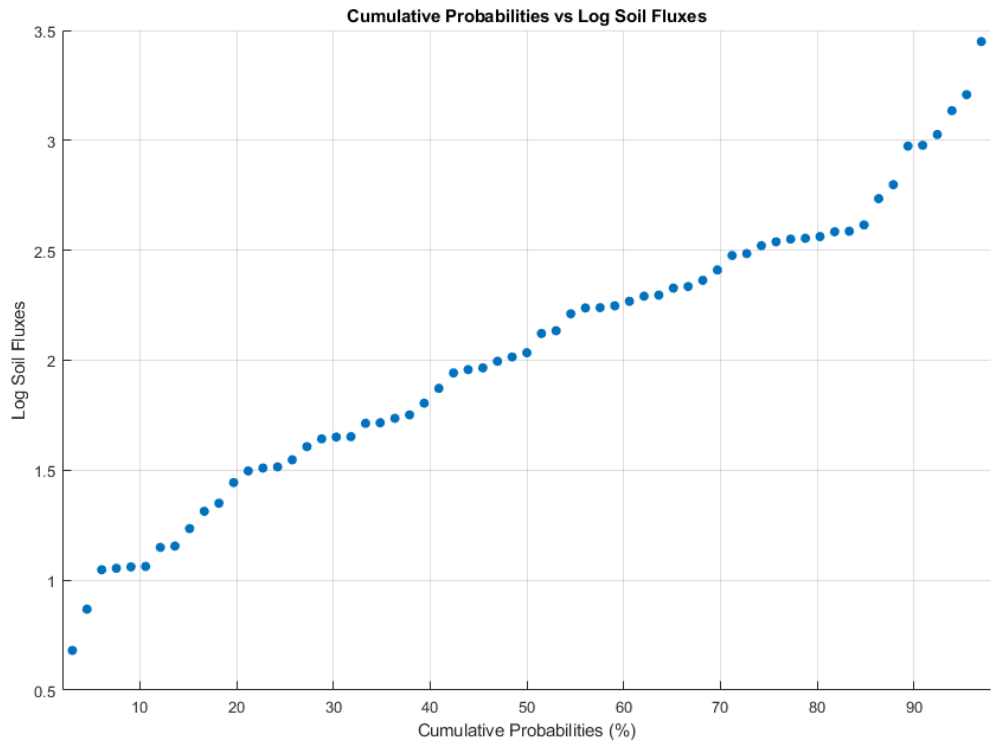


Figure 5-12 Cumulative Probabilities vs logarithm fluxes of the March 2023 soil flux measurements

The earlier soil carbon dioxide measurements carried out at Kızıldere have established a baseline for natural soil carbon dioxide emissions before reinjection. As previously mentioned, seven soil carbon dioxide flux measurements were taken prior to the carbon dioxide reinjection. The average fluxes from these surveys, along with the recent data from March 2023, are illustrated in Figure 5-13. Notably, the average post-reinjection flux aligns with seasonal trends and is situated between the flux values recorded in March 2019 and April 2019.

The comparison of point soil fluxes obtained from the March 2019 and March 2023 measurements are depicted in Figure 5-14. The fluxes from these two periods are largely similar, with a few exceptions having relatively higher differences. Variations between the fluxes can be linked to alterations in soil properties, likely influenced by agricultural activities conducted between the measurement periods, a common occurrence in the Kızıldere geothermal field.

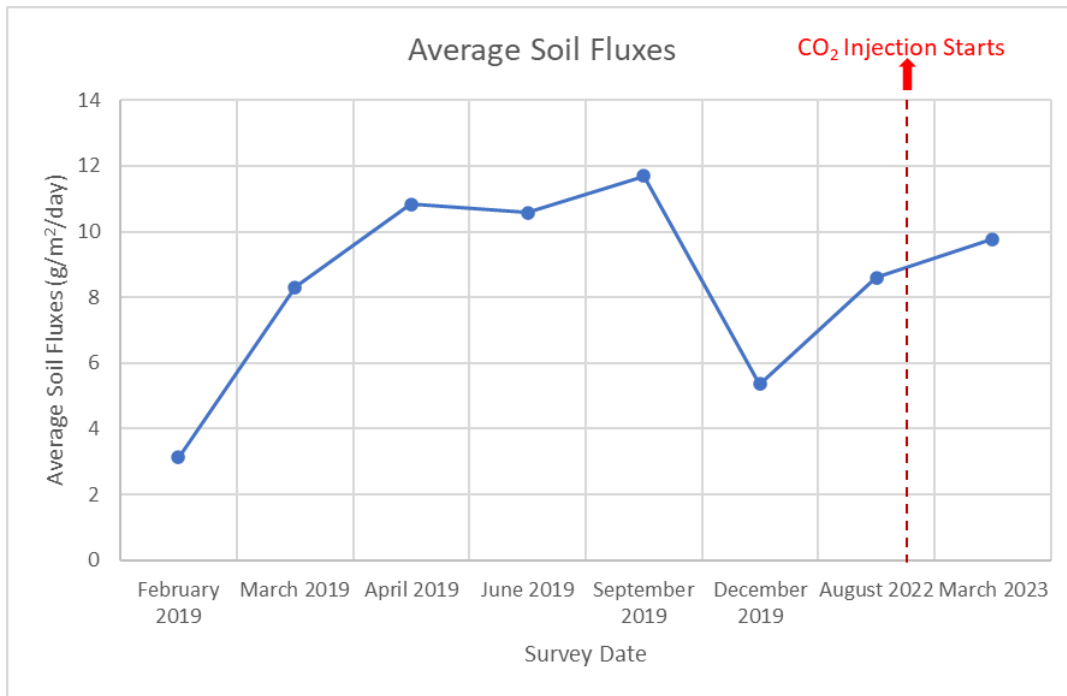


Figure 5-13 Averages of soil carbon dioxide flux measurements from Kızıldere Geothermal Field.

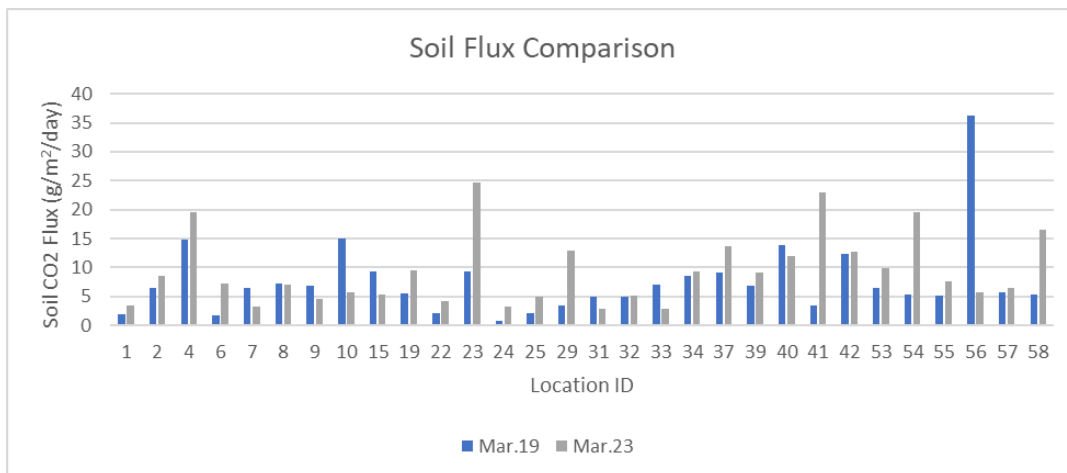


Figure 5-14 Location based comparison of soil fluxes between March 2019 and March 2023 measurements.

Another factor contributing to the differences in soil fluxes is their sensitivity to soil temperature and humidity. To explore the impact of these environmental variables, four measurement points were selected for analysis, with their respective soil temperature, relative humidity, and soil flux relationships compared. The criteria for

selecting these points were as follows: Location 1 is situated near the carbon dioxide reinjection well KD50A; Location 22 is positioned between the first fault outcrop and the reinjection well; Location 42 is at the first fault outcrop; and Location 53 is at the second fault outcrop. The corresponding plots for soil flux, temperature, and humidity for these locations are presented in Figure 5-15, Figure 5-16, Figure 5-17, and Figure 5-18.

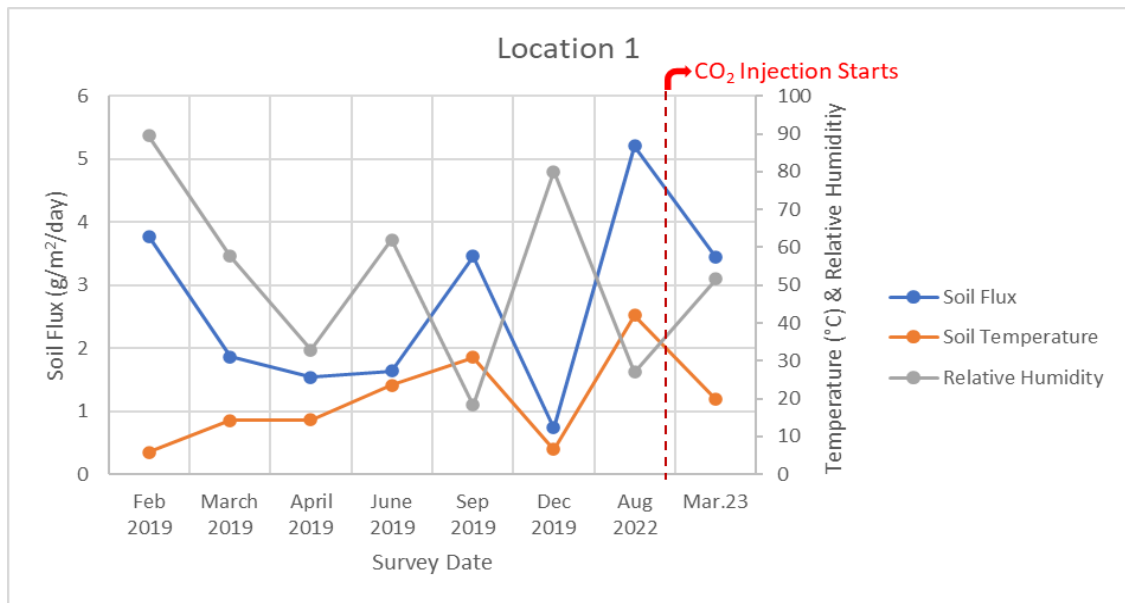


Figure 5-15 Comparison of soil flux, soil temperature and humidity measured at location 1 which is near the reinjection well.

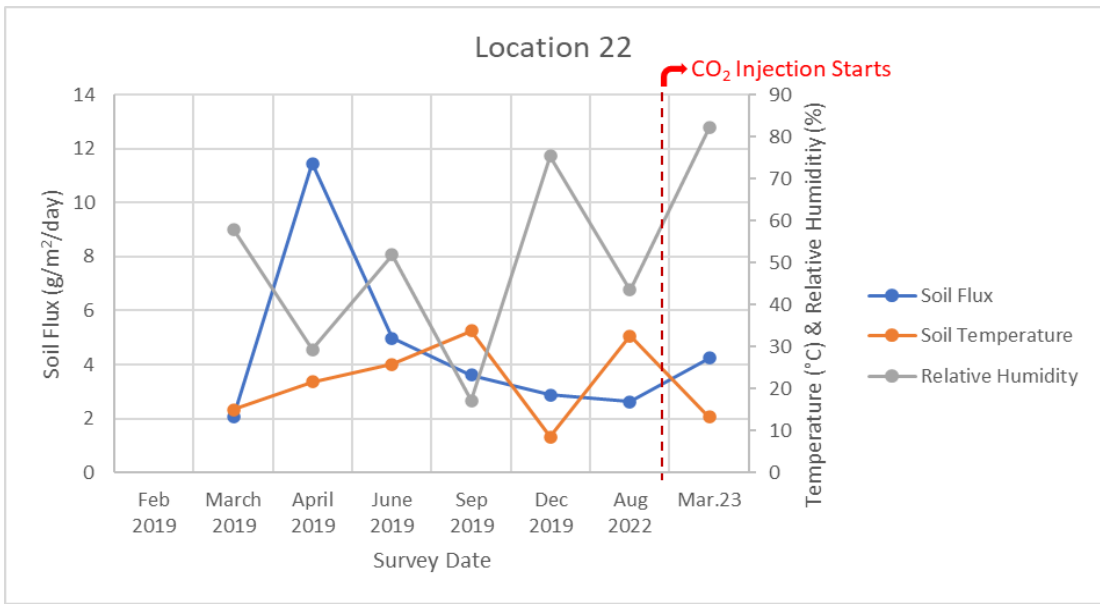


Figure 5-16 Comparison of soil flux, soil temperature and humidity measured at location 22 which is between the first fault outcrop and the reinjection well.

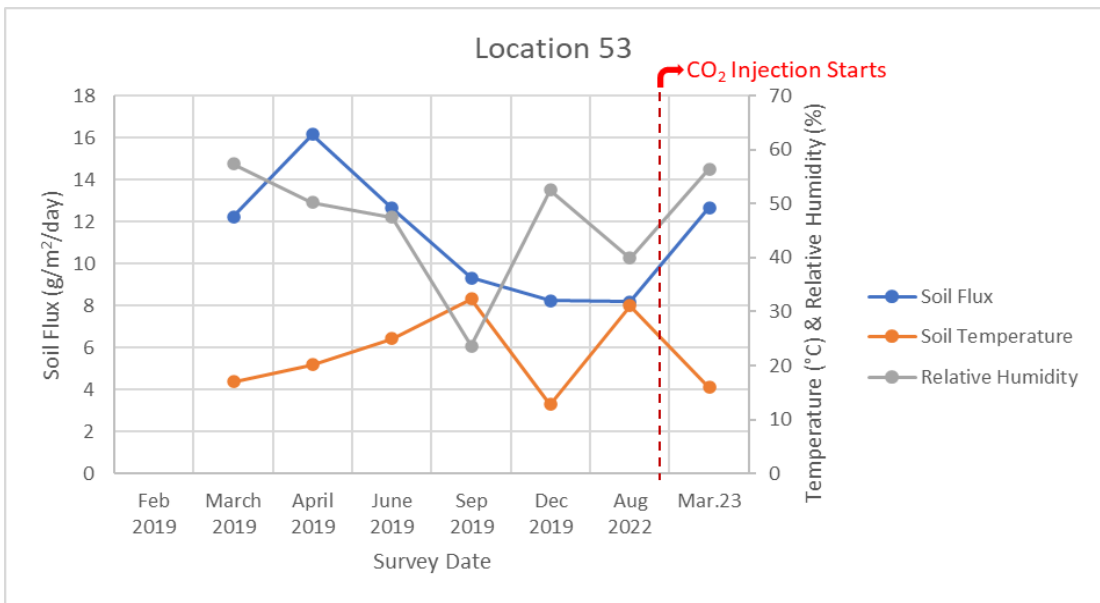


Figure 5-17 Comparison of soil flux, soil temperature and humidity measured at location 53 which is located at second fault outcrop.

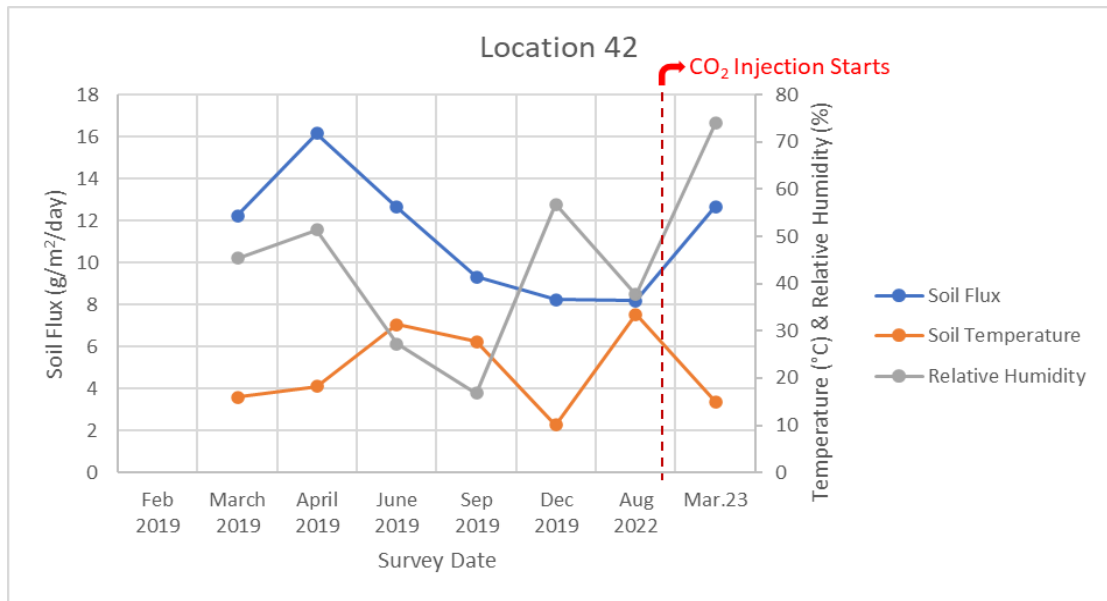


Figure 5-18 Comparison of soil flux, soil temperature and humidity measured at location 42 which is located at first fault outcrop.

In summary, the findings indicate that the soil carbon dioxide flux levels at the Kızıldere geothermal field have remained within the expected natural seasonal variations following the carbon dioxide reinjection. Consequently, it can be inferred that the reinjected carbon dioxide has not resulted in any significant increase in the soil carbon dioxide flux in the study area.

For the calibration of the soil flux parameter in the lumped parameter model, it's crucial to use only those measurements that are directly linked to the subsurface reservoir. Incorporating additional measurements that do not relate to the subsurface reservoir might lead to inaccurate calibration results, as these measurements are not reflective of the responses of subsurface conditions. To address this issue, the bimodal lognormal distribution observed in the flux measurements is partitioned into subpopulations. The partitioning process was conducted by examining logarithmic probability plots, following the procedure established by Sinclair in 1974. The partitioning is done by the following steps:

1. The logarithms of fluxes versus cumulative probabilities are plotted.
2. Inflection points on the resulting curve are identified.

3. A single inflection point shows there are two underlying subpopulations within this data.
4. For each subpopulation, individual lines are drawn with respect to the proportions determined from the inflection points.
5. Subpopulation parameters are calculated from the resulting curves for subpopulations.

The selection of inflection points in Sinclair's method can be somewhat subjective. This means that the process of partitioning the data into different populations is not entirely definitive and can vary depending on the individual interpreting the data.

For the partitioning of the flux measurement data from August 2022 and March 2023, an approach similar to the outlined by Di Martino et al. in their 2020 study is employed. Their approach is to partition the data into three populations:

1. **Background Population:** A population which is characterized by low fluxes of carbon dioxide. It represents the baseline or standard levels of CO₂ flux from the soil. This group can be related to the biogenic source of carbon dioxide.
2. **Transient Population:** This population is identified by intermediate soil flux values. It is considered a transitional or mixed group, containing elements or characteristics of both the background and the anomalous populations.
3. **Anomalous Population:** A population which has high soil flux values that can be related to volcanic or hydrothermal systems.

The partitioning of August 2022 and March 2023 soil flux surveys can be seen in Figure 5-19, Figure 5-20, respectively.

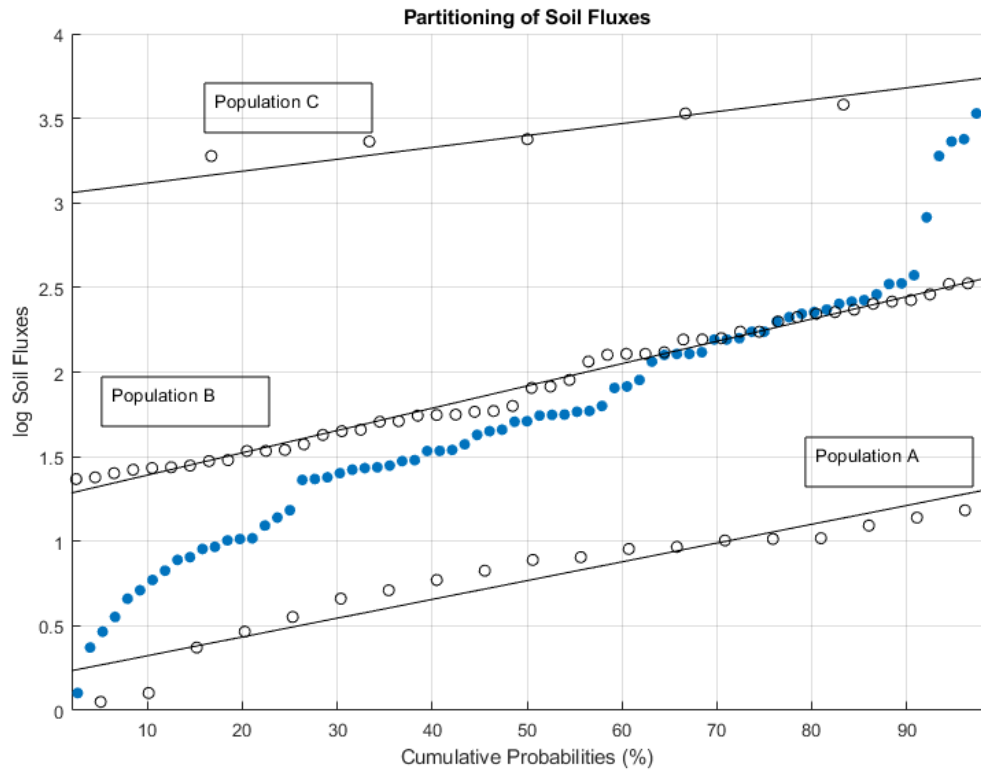


Figure 5-19 Probability plots and partitioning of August 2022 soil flux measurements.

The blue dots in Figure 5-19, and Figure 5-20 are the cumulative probabilities of soil flux measurements, black dots refer to the respective subpopulations.

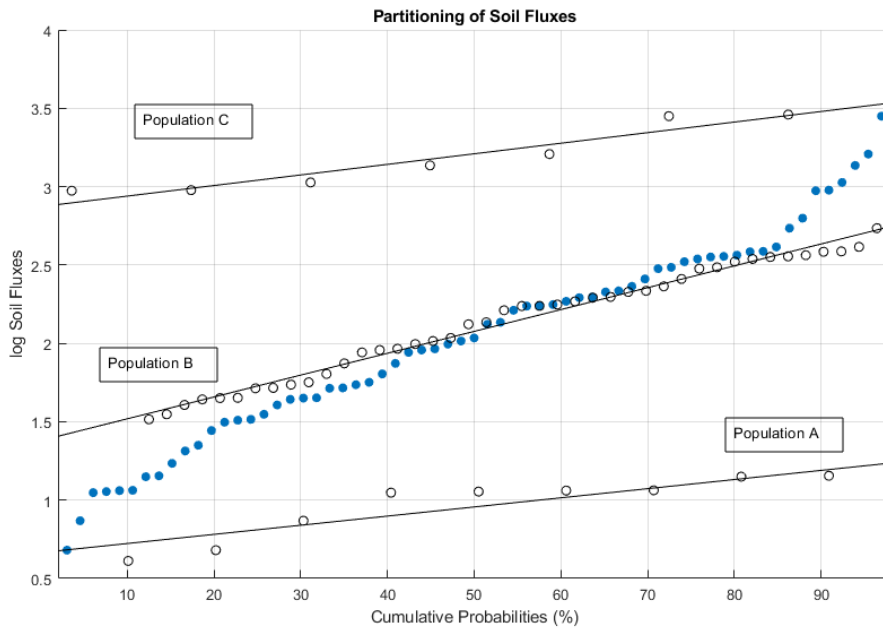


Figure 5-20 Probability plots and partitioning of March 2023 soil flux measurements.

Estimated parameters of partitioned populations for August 2022, and March 2023 soil flux surveys are given in Table 5-3, and Table 5-4, respectively.

Table 5-3 Estimated parameters of partitioned populations for August 2022 measurements.

Population	Proportion (%)	Mean (g/m ² day)
A: Background	26	1.24
B: Transient	65.8	3.52
C: Anomalous	7.9	21.05

Table 5-4 Estimated parameters of partitioned populations for March 2023 measurements.

Population	Proportion (%)	Mean (g/m ² day)
A: Background	15	1.94
B: Transient	74	3.97
C: Anomalous	11	17.68

Mean soil carbon dioxide fluxes from the Kızıldere Geothermal Field are relatively low compared to other geothermal fields reported in the literature such as: Torre Alfina, with a reported mean flux of $103 \text{ g m}^{-2} \text{ d}^{-1}$ (Carapezza et al., 2015); Larderello, reported mean flux of $197 \text{ g m}^{-2} \text{ d}^{-1}$ with record high flux measurements as high as $2927 \text{ g m}^{-2} \text{ d}^{-1}$ (Taussi et al., 2022).

The resulted anomalous populations can be associated to the fluxes sourced from the hydrothermal system subsurface as the mean values of the anomalous populations are significantly higher compared to the other populations.

The resulting anomalous populations are used to approximate soil flux rate from the study area by following formula:

$$\text{Soil Flux Rate} \left(\frac{\text{g}}{\text{day}} \right) = A \bar{x}_c \quad (25)$$

Where A is the study area (m^2), \bar{x}_c is the mean of anomalous subpopulation partitioned from lognormal distribution of soil flux measurements ($\text{g m}^{-2} \text{ day}^{-1}$).

Using the equation 25, following soil flux rates for the August 2022, and March 2023 surveys are calculated:

Table 5-5 Soil flux rates calculated from anomalous populations:

Measurement	Soil Flux Rate (kg/s)
August 2022	0.775
March 2023	0.605

The dimensionless parameter (θ) proposed for soil fluxes in the lumped parameter model is then calibrated manually to match the August 2022, and March 2023 rates. The match obtained can be seen in Figure 25.

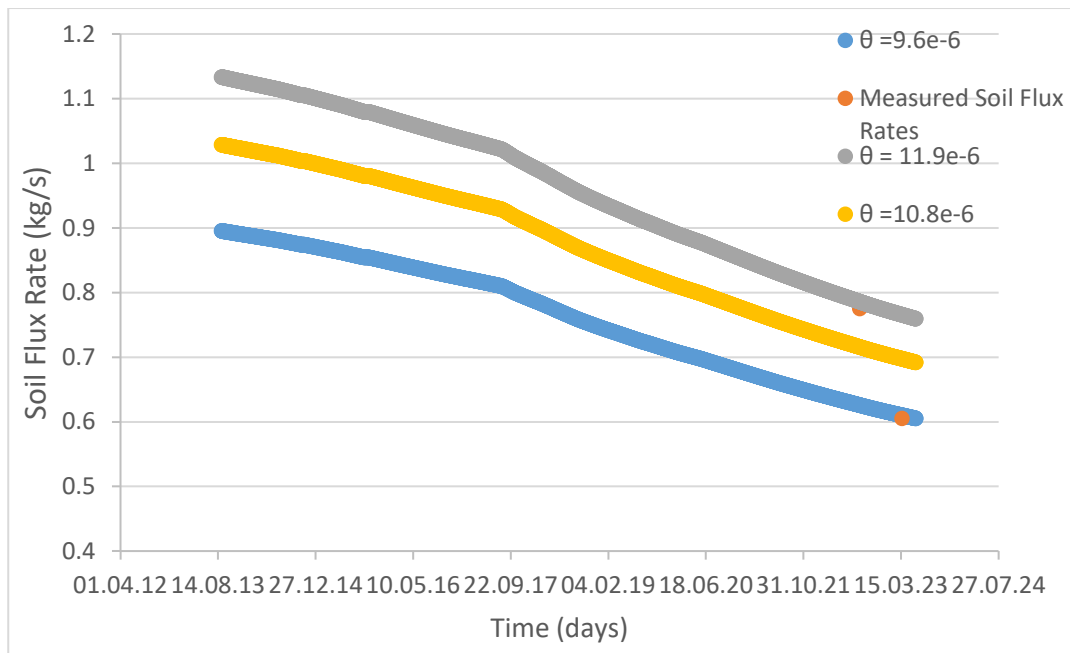


Figure 5-21 Sensitivity analysis of theta parameter for history matching of carbon dioxide soil flux rates.

The θ value resulting in the lowest root mean square error is $\theta = 10.8 \times 10^{-6}$ with error of 0.07793 compared with calculated soil flux rates. Consequently, $\theta = 10.8 \times 10^{-6}$ is selected. When comparing the soil flux rates obtained from the lumped parameter model, with the soil flux measurement rates, it's observed that they do not strictly align with the expected trend. This discrepancy can be explained by the definition of parameter θ . The parameter θ is proposed to be proportional to parameters controlling the diffusion of carbon dioxide from reservoir to surface, however, with this assumption, the effect of surface conditions such as soil type, humidity, ambient temperature, soil temperature on soil fluxes is ignored. Granieri et al. (2003) have reported that soil humidity and air temperature can explain most of the observed variances at a given location. Given that the two sets of flux rate measurements were taken in different seasons (August 2022, March 2023), each with distinct surface conditions, the deviation from the model's predicted trend is considered acceptable.

The tank parameters obtained from the history matching process are presented in Table 5-6. The matched model now can be used to make future predictions, as it can sufficiently mimic the historical data of the study area.

Table 5-6 The tank parameters obtained from the history matching process.

Bulk Volume of Tank 1, m ³	35x10 ⁸
Bulk Volume of Tank 2, m ³	1x10 ¹⁵
Porosity of Tank 1, fraction	0.13
Porosity of Tank 2, fraction	0.13
Density of rock matrix, kg m-3	2600
Specific heat capacity of the rock matrix, kJ kg ⁻¹ C ⁻¹	1000
Recharge index, kg bars ⁻¹	27.5
Soil flux parameter θ	10.8x10 ⁻⁶
Initial Pressure of Tank 1, bars	158
Initial Pressure of Tank 2, bars	158
Initial Temperature of Tank 1, C	212
Initial Temperature of Tank 2, C	212
Initial mass fraction of carbon dioxide of Tank 1, fraction	0.021
Initial mass fraction of carbon dioxide of Tank 2, fraction	0

5.3 Scenarios on Carbon Dioxide Reinjection

In this section, the calibrated model is employed to investigate three different scenarios related to carbon dioxide reinjection in the Kızıldere Geothermal Field. Three scenarios are investigated: the first scenario, where no carbon dioxide is reinjected to the study area; the second scenario, which involves reinjecting water with 1 weight percent of carbon dioxide; the third scenario where the produced carbon dioxide mass fraction is equal to the injected carbon dioxide mass fraction. For each of the mentioned scenarios, simulations are done with lumped parameter model developed over a period of five years to compare the carbon dioxide content in the reservoir. In all scenarios, the net productions and reinjection rates are kept constant for the duration of the simulations. The production and reinjection rates for the scenarios are given in Figure 5-22:

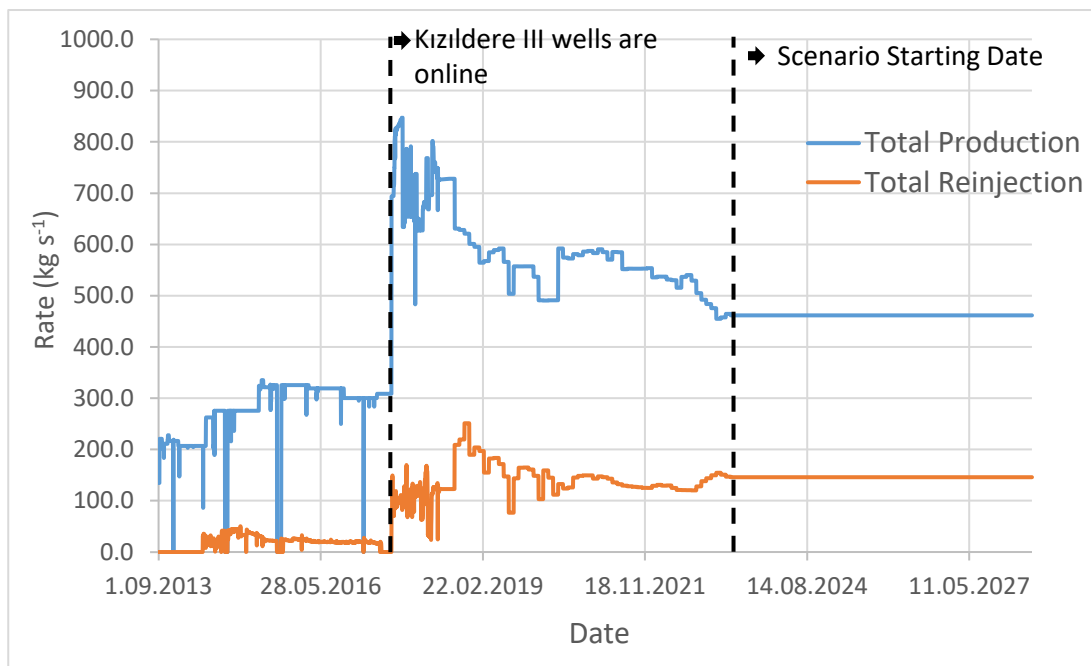


Figure 5-22 The total production and reinjection rates for the scenarios investigated.

5.3.1 Scenario 1

This scenario represents the current operating conditions of Kızıldere Geothermal Field. Although some portion of the produced carbon dioxide is reinjected back into the reservoir for approximately five months, there is currently no ongoing carbon dioxide reinjection program in the field. The net production and reinjection rates for this scenario were shown in Figure 5-22.

The mass fraction of carbon dioxide at reservoir tank after five years is plotted in Figure 5-23.

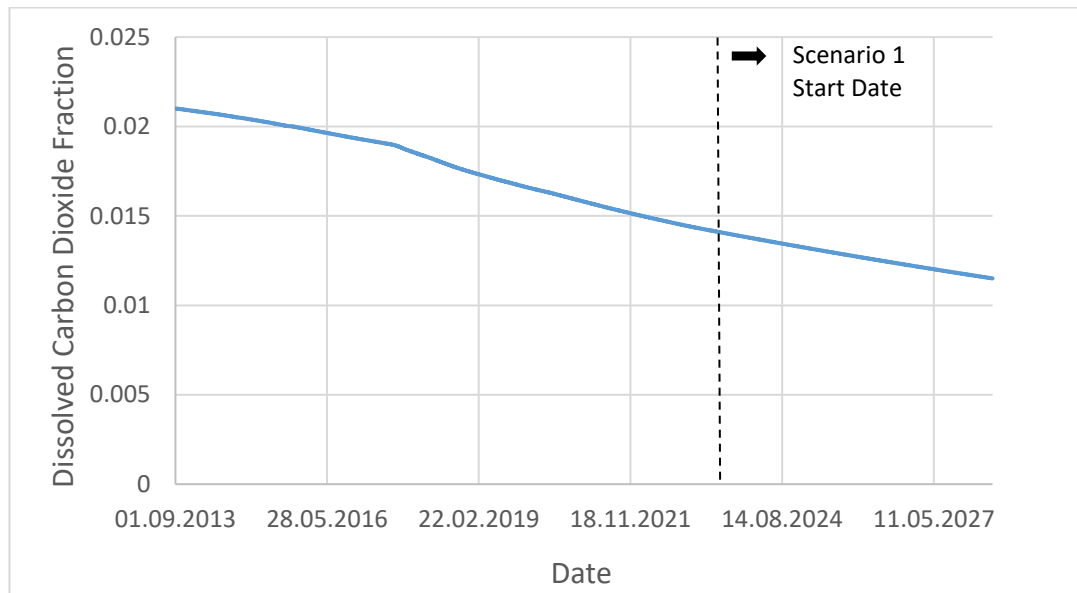


Figure 5-23 Dissolved carbon dioxide mass fraction at the reservoir after five years.

The carbon dioxide mass fraction drops to 0.0115 at the end of scenario 1. This decrease is a result of dilution caused by both reinjection of water with no carbon dioxide content and by the recharge from tank 2 to tank 1 with water having no carbon dioxide content. Soil flux rates resulting from this scenario can be seen in Figure 5-24:

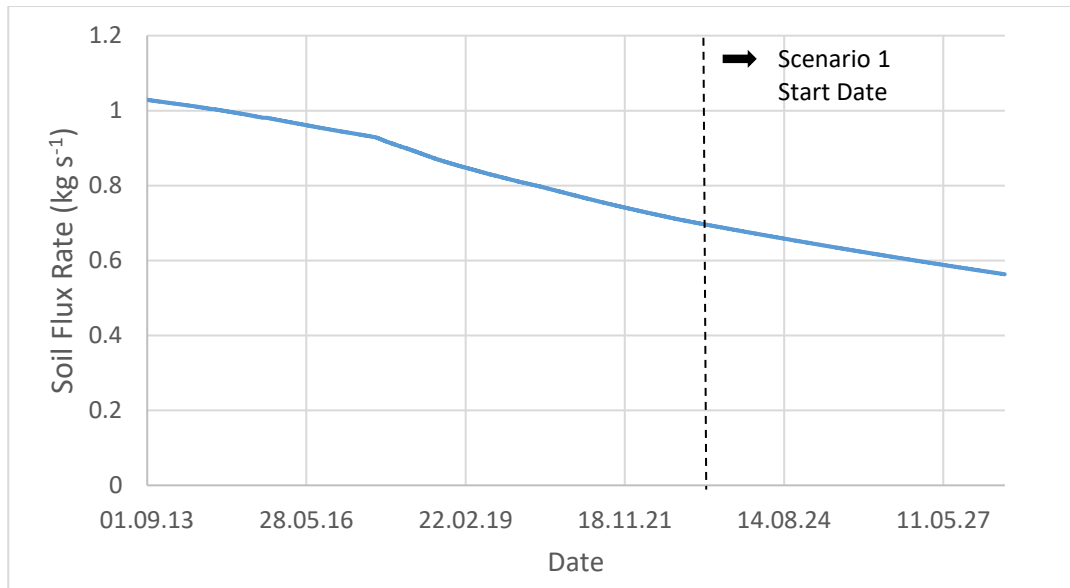


Figure 5-24 Soil flux rates out from the reservoir tanks for scenario 1.

Since the soil fluxes from the tank are directly proportional to current carbon dioxide amount of the tank, with the decrease of carbon dioxide content in the reservoir, soil fluxes from the tank also decrease.

5.3.2 Scenario 2

This scenario represents a possible scheme of carbon dioxide reinjection into Kızıldere Geothermal Field. In this scenario starting from 1.06.2023, the total reinjection is done with water having 1 weight percent of carbon dioxide. The net production and reinjection rates for this scenario were shown in Figure 5-22.

The mass fraction of carbon dioxide at reservoir tank after five years is plotted in Figure 5-25.

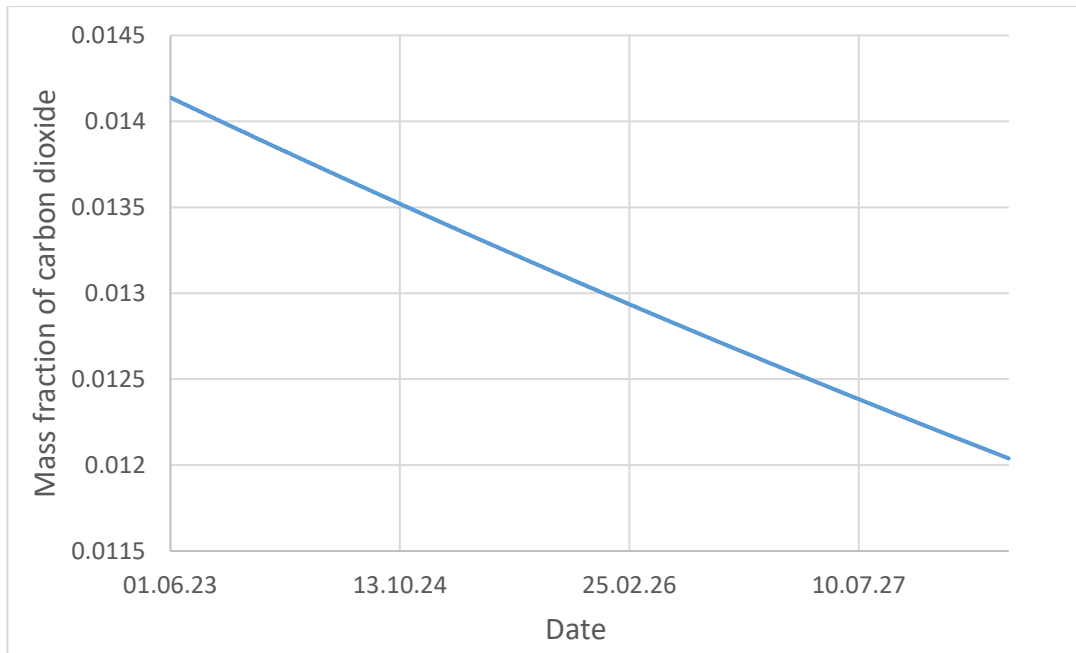


Figure 5-25 Dissolved carbon dioxide mass fraction at the reservoir after five years. The carbon dioxide mass fraction drops to 0.0120 at the end of scenario 2. This decrease is again caused by the dilution due to reinjection of water with less carbon dioxide content than the reservoir. Moreover, the recharge from tank 2 also causes further dilution since it has no carbon dioxide content. Soil flux rates resulting from this scenario can be seen in Figure 5-26.

As the soil fluxes emanating from the tank are directly proportional to the current carbon dioxide content within the tank by parameter θ , a decrease in the carbon dioxide levels in the reservoir consequently leads to a reduction in the soil fluxes from the tank.

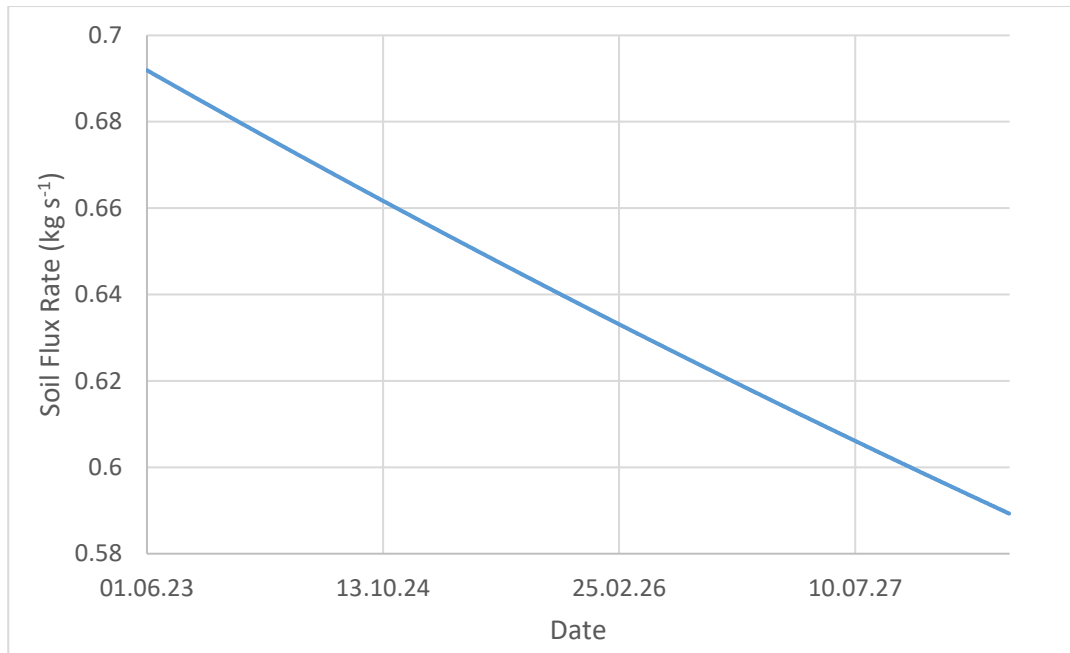


Figure 5-26 Soil flux rates from the reservoir tanks for scenario 2.

5.3.3 Scenario 3

This scenario represents another possible scheme of carbon dioxide reinjection into Kızıldere Geothermal Field. In this scenario starting from 1.06.2023, the total reinjection is done with water having 1.5 weight percent of carbon dioxide. The net production and reinjection rates for this scenario were shown in Figure 5-22.

The mass fraction of carbon dioxide at reservoir tank after five years is plotted in Figure 5-27.

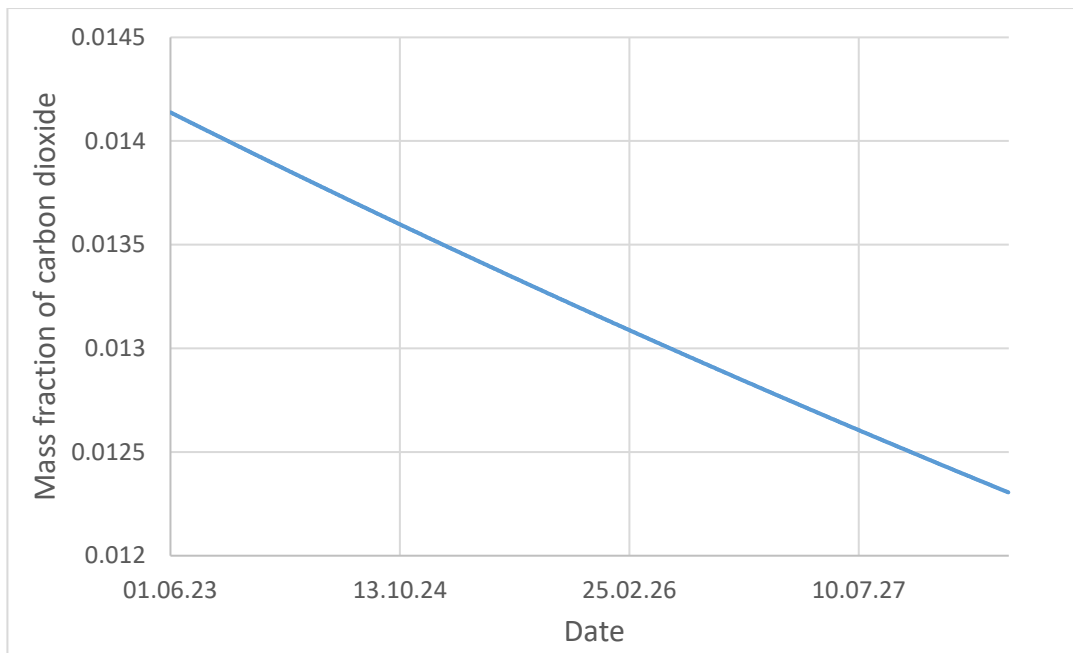


Figure 5-27 Dissolved carbon dioxide mass fraction at the reservoir after five years. The carbon dioxide mass fraction drops to 0.0123 at the end of scenario 3. Similar dilution behavior has been observed compared to scenario 2. The mass fraction of carbon dioxide at the reservoir is slightly higher than scenario 2.

Soil flux rates resulting from this scenario can be seen in Figure 5-28:

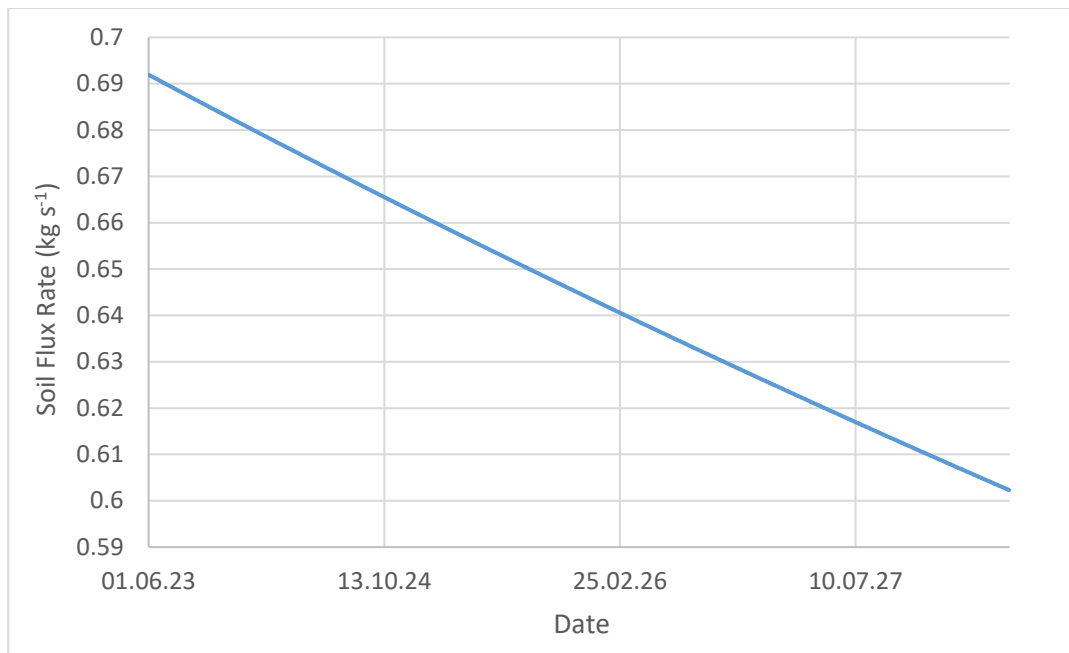


Figure 5-28 Soil flux rates out from the reservoir tank for scenario 3.

Similar to the previous results, soil flux rate decreases with decreasing carbon dioxide content in the reservoir.

The comparison of the different scenarios in terms of carbon dioxide content over the five-year period is depicted in Figure 5-29. This figure depicts how each scenario impacts the carbon dioxide levels in the reservoir over time, offering a comparative perspective of the long-term results of each carbon dioxide reinjection scenario.

Between compared strategies, Scenario 3, where the reinjection carbon dioxide mass fraction is equal to 1.5 weight percent of water, results in the highest carbon dioxide content at the end of five years. This is expected because, the recharge of carbon dioxide into the reservoir tank is only possible through reinjection of carbon dioxide. Elevated levels of carbon dioxide reinjection would result in increased carbon dioxide concentrations in the system.

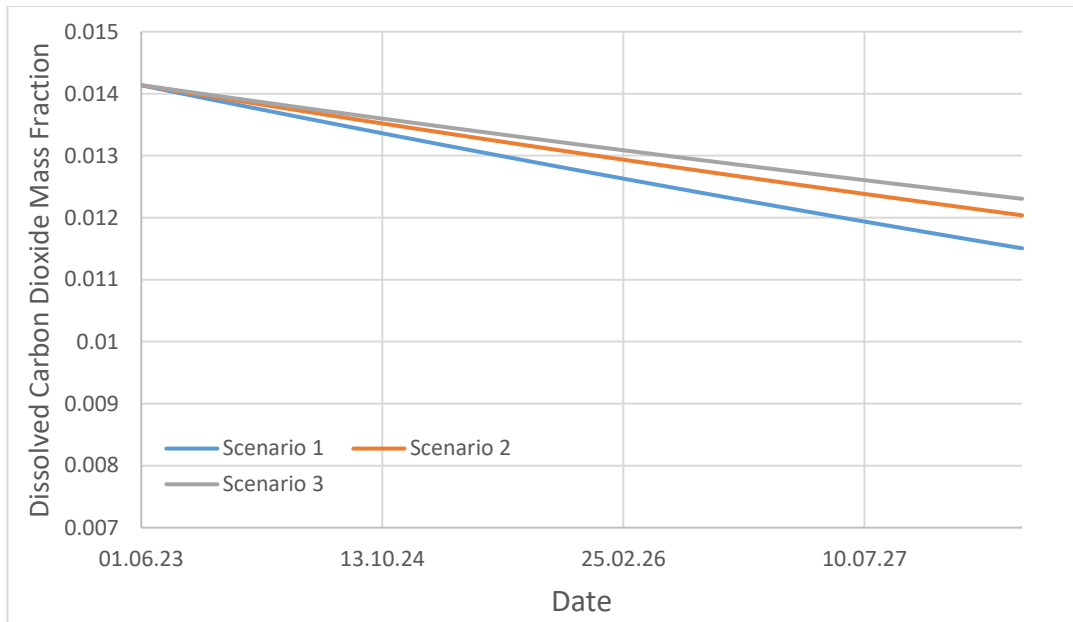


Figure 5-29 Comparison of scenarios with respect to the carbon dioxide content of the reservoir.

In all the scenarios simulated, there is a noticeable decrease of carbon dioxide content in the reservoir. The influx of fluid from tank 2, which has zero carbon dioxide concentration, and the imbalance between the amount of water produced and reinjected, both contribute to lowering of the carbon dioxide concentration in the reservoir over the simulation time. This observation is consistently seen across the different scenarios modeled in the study.

Despite the known presence of dissolved carbon dioxide in the vicinity of the study area, the history matching process revealed that the carbon dioxide mass fraction in the recharge tank is effectively zero. This indicates a strong connection between the reinjection and producer wells. The reinjected water seems to be rapidly reaching the areas near the producing wells, thereby diluting, and reducing the concentration of carbon dioxide in those regions.

CHAPTER 6

CONCLUSIONS AND FUTURE REMARKS

A generalized lumped parameter model that can account for soil fluxes is presented in this study. To predict pressures, temperatures, and carbon dioxide mass fractions, conservation of mass and energy principles are applied. The developed model allows any number of tanks each can have different number of connections. This comes in handy when complex geothermal reservoirs needed to be simulated using a lumped parameter model. The developed model proposes a parameter (θ) which quantifies the amount of soil flux that will be emanating from the tank given the carbon dioxide amount. This proposed parameter is a representation of diffusion of carbon dioxide from reservoir to surface.

Kızıldere Geothermal Field has been chosen as one of the demonstration sites of the GECCO project, due to its naturally high content of carbon dioxide. As part of this project, some portion of the produced carbon dioxide has been reinjected into the geothermal reservoir. To assess the safety and feasibility of the pilot carbon dioxide reinjection, a monitoring campaign has been initiated. As part of this monitoring campaign, soil flux measurements at Kızıldere Geothermal Field have been collected similar to other carbon capture and storage (CCS) sites around the world.

The developed lumped parameter model is applied to a sector that contains the wells near the pilot carbon dioxide reinjection well KD50A. The model consists of two tanks - a recharge source tank and a reservoir tank. Historical data on production and reinjection from September 1, 2013, to June 1, 2023, were used for history matching. The accuracy of the pressure matches was assessed by comparing them with the observation data from the well KD50A. The θ parameter calibration was based on soil flux rates derived from two soil flux surveys. The soil flux rates are calculated by partitioning the soil flux measurements into subpopulations of anomalous,

transient, and background and identifying individual subpopulation parameters. The proportion of anomalous subpopulation for August 2022 and March 2023 measurements were 7.9%, and 11% respectively.

As a result of history matching process, recharge constant between recharge and the reservoir tank is determined to be $27.5 \text{ kg bar}^{-1}\text{s}^{-1}$. Soil flux parameter θ is determined to be 10.8×10^{-6} . Bulk volume of the reservoir tank is selected as $35 \times 10^8 \text{ m}^3$. Initial mass fraction of carbon dioxide in recharge tank is determined to be 0.

Upon the completion of history matching, a model that is capable of simulating the sector model area is obtained. The obtained model then used to make predictions for upcoming five years with three different carbon dioxide reinjection strategies. The first strategy is to not the reinject any carbon dioxide. Carbon dioxide content of the reservoir tank decreases to 0.0115 after five years with this strategy. In the second scenario, involving the reinjection of water with 1 weight percent carbon dioxide, the content decreases to 0.0121. In the third strategy, where water containing 1.5 weight percent of carbon dioxide is reinjected, the model predicts that the carbon dioxide content in the reservoir tank will reach 0.0123 after a period of five years.

In each of the reinjection scenarios analyzed, a dilution of carbon dioxide in the study area was observed. This reduction in carbon dioxide concentration is primarily due to two factors. First, the net difference between the rates of reinjection and production decreases the overall amount of carbon dioxide in the system. Second, the water recharged from the recharge tank into the reservoir tank lacks carbon dioxide, which further contributes to the dilution of the carbon dioxide content in the study area. These two factors combined result in a consistent decrease in carbon dioxide levels across all the scenarios examined.

The developed lumped parameter model offers valuable insights for a proposed carbon dioxide reinjection scheme. However, it's important to recognize that this model alone is not sufficient for planning and executing such an operation. Key factors like injectivity and operational parameters, including wellhead pressures, are not accounted for in the lumped parameter model. These aspects are crucial for the

practical implementation and effectiveness of a reinjection strategy and must be considered alongside the insights provided by the lumped parameter model for a comprehensive and realistic planning process.

Future enhancements to the model presented in this thesis could focus on refining the θ parameter to better represent the influence of surface conditions on soil carbon dioxide fluxes. Given that ambient surface conditions, such as temperature, humidity, and soil type, can significantly account for variations in soil carbon dioxide flux at a specific location, incorporating these factors into the θ parameter would make the model more accurate and representative of real-world conditions.

REFERENCES

- Akın, S., Akın, T., Tokel, A. B., Erol, S., & Sevindik, B. (2023). Deliverable 7.3: Report on Chemistry of Injected Gas and Water, Report on Monitoring Results Based on Monitoring Plan from WP2, and Lessons Learned from the Demonstration [Unpublished report].
- Akın, S., Örüçü, Y., & Fridriksson, T. (2020). Characterizing the Declining CO₂ Emissions from Turkish Geothermal Power Plants. In Proceedings of the Stanford Geothermal Workshop (Vol. 45, pp. 1-9). California, United States of America, February 10-12, 2020.
- Akyapı, E. (2011). A New Non-Isothermal Tank Model for Liquid Dominated Geothermal Reservoirs. Istanbul Technical University.
- Altıkat, S., Küçükerdem, H. K., & Altıkat, A. (2019). The response of CO₂ Flux to Soil Warming, Manure Application and Soil Salinity. *Journal of the Institute of Science and Technology*, 1334-1342.
- Arps, J. J. (1945). Analysis of Decline Curves. *Transactions of the AIME*, 160(01), 228–247. <https://doi.org/10.2118/945228-G>
- Axelsson, G. (1989). Simulation of pressure response data from geothermal reservoir by lumped parameter models. Proceedings of the 14th Workshop on Geothermal Reservoir Engineering, 257-263, Stanford University, USA.
- Axelsson, G., Björnsson, G., & Quijano, J. E. (2005). Reliability of Lumped Parameter Modeling of Pressure Changes in Geothermal Reservoirs. Proceedings of the World Geothermal Congress 2005, Antalya, Turkey, 24-29 April 2005.
- Alpaslan, M. 2007. Early to Middle Miocene Intracontinental basaltic volcanism in the northern margin of the Arabian Plate, SE Anatolia, Turkey: geochemistry and petrogenesis. *Geological Magazine*. 144 (5), 867-882.

- Atkinson, P., Miller, F. G., Marconcini, R., Neri, G., & Celati, R. (1978). Analysis of reservoir pressure and decline curves in Serrazzano zone, Larderello geothermal field. *Geothermics*, 7(2–4), 133–144. [https://doi.org/10.1016/0375-6505\(78\)90004-4](https://doi.org/10.1016/0375-6505(78)90004-4)
- Camarda, M., De Gregorio, S., Capasso, G., Di Martino, R., Gurrieri, S., & Prano, V. (2019). The monitoring of natural soil CO₂ emissions: Issues and perspectives. *Earth-Science Reviews*, 102928.
- Carapezza, M., M., R., Gattuso, A., Pagliuca, N., & Tarchini, L. (2015). The sealing capacity of the cap rock above the Torre Alfina geothermal reservoir (Central Italy) revealed by soil CO₂ flux investigations. *Journal of Volcanology and Geothermal Research*, 25-34.
- Carman, C.H., Locke II, R.A. & Blackey C.S. (2014). Update on Soil CO₂ Flux Monitoring at the Illinois Basin – Decatur Project, USA. *Energy Procedia*, 63, 3869-3880. <https://doi.org/10.1016/j.egypro.2014.11.417>.
- Carman, C.H., Locke II, R., & Korose, P. (2019). Illinois Basin – Decatur Project: Soil Carbon Dioxide Flux Monitoring. Illinois State Geological Survey Circular
- Cardellini, C., Chiodini, G., & Frondini, F. (2003). Application of stochastic simulation to CO₂ flux from soil: Mapping and quantification of gas release. *Journal of Geophysical Research*, 108(B9), 2425
- Castanier, L. M., Sanyal, S. K., & Brigham, W. E. (1980). A practical analytical model for geothermal reservoir simulation. In *Proceedings of the 50th Annual California Regional Meeting of the Society of Petroleum Engineers (SPE 8887)*, 1-6. Los Angeles, CA, USA, April 9-11.
- Chiodini, G., Cioni, R., Guidi, M., Raco, B., & Marini, L. (1998). Soil CO₂ flux measurements in volcanic and geothermal areas. *Applied Geochemistry*, 13(5), 543-552.
- Chiodini, G., Frondini, F., & Raco, B. (1996). Diffuse emission of CO₂ from the Fossa crater, Vulcano Island (Italy). *Bulletin of Volcanology*, 58, 41–50.

- Di Martino, R. M. R., Capasso, G., Camarda, M., De Gregorio, S., & Prano, V. (2020). Deep CO₂ release revealed by stable isotope and diffuse degassing surveys at Vulcano (Aeolian Islands) in 2015–2018. *Journal of Volcanology and Geothermal Research*, 401, Article 106972. <https://doi.org/10.1016/j.jvolgeores.2020.106972>
- Fridriksson, T., Mateos, A., Audinet, P., & Orucu, Y. (2016). *Greenhouse Gases from Geothermal Power Production*. World Bank, Washington, DC.
- Gokcen, G., Ozturk, H. K., & Hepbasli, A. (2004). Overview of Kizildere Geothermal Power Plant in Turkey. *Energy Conversion and Management*, 45(1), 83-98.
- Granieri, D., Chiodini, G., Marzocchi, W., & Avino, R. (2003). Continuous monitoring CO₂ soil diffuse degassing at Phlegraen Fields (Italy): Influence of environmental and volcanic parameters. *Earth and Planetary Science Letters*, 167-179.
- Hoşgör, F. B. (2016). *A New Lumped Parameter (Tank) Model for Reservoirs Containing Carbon Dioxide*. Istanbul Technical University.
- Kaya, T., & Kindap, A. (2009). Kızıldere – New Geothermal Power Plant in Turkey: 1. Stage 60 MWe Turkey's Biggest Geothermal Electricity Plant Development Project. Privatization of Kızıldere Geothermal Power Plant and Current Approaches for the Field & Plant. *International Geothermal Days, Slovakia*.
- Küçük, S., Başer, A., Saraçoğlu, Ö., Akın, T., Şentürk, E., Tüzen, M., & Akın, S. (2021). Soil CO₂ Flux and Temperature Measurements in Kızıldere Geothermal Field. *Proceedings World Geothermal Congress 2020+1*. Reykjavik, Iceland.
- LICOR Biosciences. (2015). Using the LI-8100A Soil Gas Flux System and the LI-8150 Multiplexer. Retrieved from <https://www.licor.com/documents/jtpq4vg358reu4c8r4id>.

- LICOR Biosciences. (2021). SoilFluxPro Software Instruction Manual. Retrieved from <https://www.licor.com/documents/uh3tbaw1frnwca9tkl7og9uqs27j>.
- Madsen, R., Xu, L., Claasen, B., & McDermitt, D. (2009). Surface Monitoring Method for Carbon Capture and Storage Projects. *Energy Procedia*, 2161-2168.
- Morris, C. W., & Campbell, D. A. (1981). Geothermal Reservoir Energy Recovery: A Three-Dimensional Simulation Study of the East Mesa Field. *J Pet Technol*, 33, 735-742. <https://doi.org/10.2118/8229-PA>
- Olsen, G. (1984). Depletion modeling of liquid dominated geothermal reservoir. Technical Report SGP-TR-80, Stanford Geothermal Program, Stanford University, Palo Alto, California.
- Onur, M., Sarak, H., Tureyen, O.I., Cinar, M., & Satman, A., (2008). A new non-isothermal lumped parameter model for low temperature, liquid dominated geothermal reservoir and its applications. *Proceedings 33rd Workshop on Geothermal Reservoir Engineering*, Stanford University, USA.
- Pruess, K. (1991). TOUGH2-A General-Purpose Numerical Simulator for Multiphase Fluid and Heat Flow (LBNL Report #: LBL-29400). Lawrence Berkeley National Laboratory.
- Ripperda, M, & Bodvarsson, G S. (1987). Decline curve analysis of production data from The Geysers geothermal field. United States.
- Schilthuis, R. J. (1936). Active oil and energy. *Transactions of the American Institute of Mining, Metallurgical, and Petroleum Engineers*, 118, 33-52.
- Şentürk, E., & Akın, T. (2021, April). Unlocking the NCG Utilization Potential of Turkish Geothermal Fields: Criteria of Selection NCG Injection Well for GECO Project, Kizildere Geothermal Field. In *Proceedings of the World Geothermal Congress 2020+1*. Reykjavik, Iceland.

- Şimşek, Ş., Parlaktuna, M., & Akın, S. (2009). Data Gathering and Evaluation of the Kızıldere Geothermal Field. Unpublished report prepared for Zorlu.
- Şimşek, Ş., Yıldırım, N., & Gülgör, A. (2005). Developmental and environmental effects of the Kızıldere Geothermal Power Project, Turkey. *Geothermics*, 34(2), 234-251.
- Sbrana, A., Lenzi, A., Paci, M., Gambini, R., Sbrana, M., Ciani, V., & Marianelli, P. (2021). Analysis of natural and power plant CO₂ emissions in the Mount Amiata (Italy) volcanic–geothermal area reveals sustainable electricity production at zero emissions. *Energies*, 14(15), 4692.
- Sinclair, A.J. (1974). Selection of threshold values in geochemical data using probability graphs. *Journal of Geochemical Exploration*, 3, 129-149.
- Szizybalski, A., Zimmer, M., Pilz, P., & A., L. (2017). Results from twelve years of continuous monitoring of the soil CO₂ Flux at the Ketzin CO₂ storage pilot site, Germany. *Energy Procedia*, 543-548.
- Taussi, M., Brogi, A., Liotta, D., Nisi, B., Perrini, M., Vaselli, O., Zombrano, M., & Zucchi, M. (2022). CO₂ and heat energy transport by enhanced fracture permeability in the Monterotondo Marittimo-Sasso Pisano transfer fault system (Larderello Geothermal Field, Italy). *Geothermics*, 102531.
- Tokel, A., Akın, S., Akın, T., Erol, S., & Sevindik, D. (2023). Recent Soil Carbon Dioxide Flux Measurements at Kızıldere Geothermal Field. *Proceedings 48th Workshop on Geothermal Reservoir Engineering*. Stanford, California.
- Whiting, R. L., & Ramey, H. J. (1969). Application of Material and Energy Balances to Geothermal Steam Production. *Journal of Petroleum Technology*, 21(07), 893–900. <https://doi.org/10.2118/1949-PA>

Xu, T., Sonnenthal, E., Spycher, N., & Pruess, K. (2006). TOUGHREACT—A simulation program for non-isothermal multiphase reactive geochemical transport in variably saturated geologic media: Applications to geothermal injectivity and CO₂ geological sequestration. *Computers & Geosciences*, 32(2), 145–165. <https://doi.org/10.1016/j.cageo.2005.06.014>